Utrecht University

Utrecht University

Bachelor thesis

Feasibility study of the detection of higher D^* meson states with ALICE at LHC

Djin Kastje
Student number: 6262171
Faculty of Science

Supervised by
Dr. Alessandro Grelli
Syaefudin Jaelani

June 12, 2020

Abstract

Shortly after the big bang happened, a phase of matter called the quark gluon plasma (QGP) was created. This is a plasma where the constituents of nucleons roam freely instead of being bound tightly into particles. The QGP is researched at the Large Hadron Collider at CERN in an experiment called ALICE (A Large Ion Collider Experiment) where at high energies, protons and heavy ions are collided.
Mesons made up of heavy quarks such as the charm and bottom quark can be used to probe the QGP. Heavy quarks are produced in the early stages of heavy ion collisions and thus journey through the QGP's full evolution. In previous years, the J/ψ ($c\bar{c}$) and Υ ($b\bar{b}$) mesons have been used as a temperature probe. In this thesis we proposed the possibility to use higher D^* meson states, in order to investigate the maximum QGP temperature. Therefore the feasibility of the detection of $D^*(2010)^+$, $D_0^*(2400)^0$, $D_1(2420)^0$ and $D_2^*(2460)^0$ was investigated. Simulations of 10 million pp collisions were executed at a center of mass energy of 13 TeV using ROOT and PYTHIA. The results showed that, depending on the species, we can expect a range of a few millions to a few billions of D mesons produced within ALICE detector acceptance $|\eta| < 0.9$. Such numbers give a reasonably safe number of D mesons in order to perform the reconstruction in LHC run III data sample. Furthermore, evidence was provided that we cannot aim, in data, to reconstruct the higher D^* meson states below a p_T of 1-2 GeV/c due to intrinsic limits on the ALICE low p_T tracking.

Contents

Chapter 1

Introduction and motivation

When you look up the website of CERN, the first thing that catches your eye are the big lettered questions "What is the nature of the universe? What is it made of?" [5]. These capture some of humanities most fundamental questions and have been asked throughout history. Already in the 5^{th} century BC curiosity about matter led to ideas and theories hinting at the existence of smaller particles [23]. Nevertheless, they remained theoretical for approximately another 2500 years [15]. A more systematic way of finding answers to these questions is to go all the way back to the big bang. Shortly after the big bang happened, a phase of matter called the quark gluon plasma (QGP) was created. This is a plasma where the constituents of nucleons roam freely instead of being bound tightly into particles. However, when the temperature dropped, these partons formed into the stable protons, neutrons and other composite particles we now see in nature. To research this primordial matter and how the matter we know came into existence, we need to recreate this QGP.

The quark gluon plasma is researched at the Large Hadron Collider at CERN in an experiment called ALICE (A Large Ion Collider Experiment) where at high energies, protons and heavy ions are collided. The temperature and density reached in one such heavy-ion collision is high enough to produce a small droplet of QGP. By measuring the momenta of the final particles which are detected by ALICE's detectors, reconstructing the tracks of tens of thousands of these final particles, identifying the particles by their interaction with specific parts of the detector and observing the decay vertices of heavy charm and bottom quarks, the properties of the plasma are investigated.

One interesting property of the QGP is its temperature. The QGP only exists for about 10^{-23} seconds and it is expected to be a few hundreds of thousand times hotter

than the core of the sun [27]. This makes it difficult to use a "conventional" thermometer. Instead, certain particles can be used to probe the QGP in order to reconstruct its temperature. Heavy quarks such as the charm and bottom quark are particularly fit for this goal. They are produced in the early stages of the heavy ion collisions and thus journey through the QGP's full evolution. In previous years, the J/ψ ($c\bar{c}$) and Υ ($b\bar{b}$) mesons have been used as a probe [19] [27].

In this thesis we investigate a new idea: the possibility to use D mesons to investigate the maximum temperature of the plasma. They differ from the earlier mentioned mesons as they only have one charm quark and a differently flavoured anti-quark. The various D meson states are characterized by a unique Debye length or bounding energy. When they journey through the QGP, they experience colour screening. If the effect of the colour screening is larger than the effect of the binding energy, the D meson will melt. Mesons that are more weakly bound thus melt earlier in the QGP than stronger bound mesons, which enables us to examine the temperature of the QGP.

In the coming chapters the feasibility of the detection of $D^*(2010)^{+-}$, $D_0^*(2400)^0$, $D_1(2420)^0$ and $D_2^*(2460)^0$ will be investigated. First we will delve into the theory behind the Quark Gluon Plasma. ALICE's detector is discussed next. Afterwards, the methodology for this thesis is explained followed by its results, conclusion and outlook for the future.

Chapter 2

Theoretical framework

In order to better understand why we want to research $D^*(2010)^+$, $D_0^*(2400)^0$, $D_1(2420)^0$ and $D_2^*(2460)^0$ and study their kinematic properties, we first need to look into the theoretical background. In the following sections, we will further dive into the standard model, quantum chromodynamics (QCD), the quark gluon plasma (QGP) and suppression and regeneration in the QGP. Lastly, I will introduce $D^*(2010)^+$, $D_0^*(2400)^0$, $D_1(2420)^0$ and $D_2^*(2460)^0$ in more detail.

2.1 Standard model

Fundamental or elementary particles called partons and leptons are what we currently consider to be the smallest existing particles in the universe. The standard model describes these particles and three out of the four forces, namely the electromagnetic, strong and weak force. The gravitational force is excluded. As can be seen in figure 2.1, the standard model groups the elementary particles into two categories, fermions and bosons. Fermions are regarded as being the matter particles and bosons as being the interaction particles.

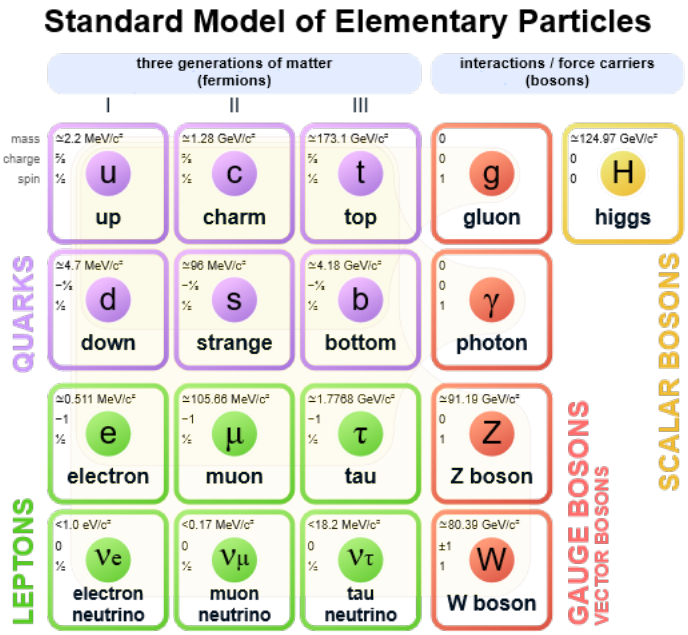

Figure 2.1: Standard Model of Elementary Particles [29]

We will start with discussing the fermions, the matter particles. The fermions are half-integer spin particles, which means that their intrinsic angular momentum is quantified in half-integers. The fermions can be further split into quarks and leptons. There are three generations of leptons. In the first generation we have the electron with corresponding neutrino ν_e, the muon with ν_μ in the second and the tau with ν_τ in the third and all their respective antiparticles. Leptons are particles that are described by the electromagnetic force with the exception of the neutrinos which only feel the weak force. The three generations are grouped according to their charge (Q), electron number (L_e), muon number (L_μ) and tau number (L_τ).

Quarks, on the other hand, are described by the strong force. Similar to the leptons, the six quarks are also split into three families. The first generation consists of quark flavour down (d) and up (u), the second of strange (s) and charm (c) and the third of bottom (b) and top (t). Again quarks also have their antiparticles, antiquarks. The quarks are grouped according to their charge, upness (U), downness (D), strangeness (S), charm (C), beauty (B), and truth (T).

Bosons are particles with integer spin. They are also split into two types, namely the gauge bosons and the scalar bosons. The first are interaction particles and are, as the

name already says, responsible for mediating interactions. The electromagnetic force is mediated by the photon (γ), the weak force by the three bosons W^{+-} and Z^0, the strong force by the gluon (g) and gravity supposedly by the graviton, although this particle remains to be observed. Currently, there is only one known scalar boson, the Higgs boson, first observed in 2012 [9]. The Higgs boson has zero spin and is described by the Higgs field. This is a complex scalar field. In constrast to the gauge bosons, these are described by gauge fields which are usually vector fields.

2.2 Quantum Chromo Dynamics

The strong interactions are described by the theory of quantum chromodynamics (QCD). Similar to the role of electrical charge in QED, colour charge is conserved in QCD in all physical processes. There are three types of colour charges. By convention, these are red, green and blue. The particles that carry this colour charge are quarks. Furthermore, where electrical charges are mediated by the massless photon, colour charges are mediated by the massless gluon. Gluons, however, also carry colour charge themselves. This enables them to interact with each other, as opposed to photons who cannot. Together, the gluons form the color-SU(3) octet, where the eight different gluons carry different combinations of the colour charges. The ninth combination is not in the octet as it does not occur in nature.

There are two important phenomena in QCD, namely asymptotic freedom and colour confinement. In QCD the coupling constant is given by α_s and behaves as can be seen in figure 2.2. For low momentum transfer (Q), the coupling constant is high and it decreases as Q increases. In other words "hard" quarks whose energy and momentum is high, couple weakly, whereas "soft" quarks with low energy and momentum, couple strongly. Asymptotic freedom thus describes the decrease of the running coupling constant with increasing energy and momentum.

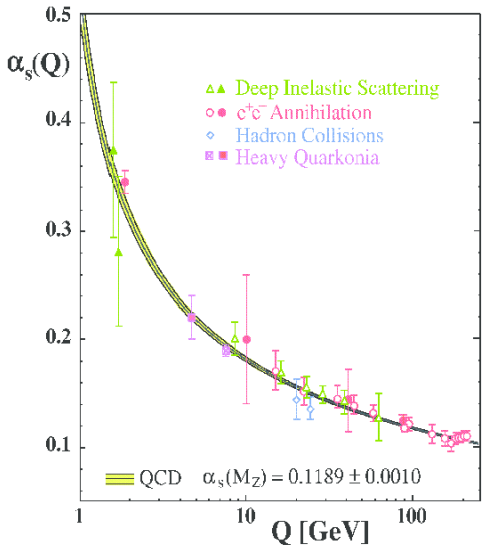

Figure 2.2: The strong coupling constant is plotted against the momentum transfer. It shows the concept of asymptotic freedom. [8]

Colour confinement follows from asymptotic freedom. If colour carriers such as quarks are close to each other, they feel no pull, as predicted by asymptotic freedom. However, if say a bounded quark and antiquark are pulled apart, the strong force increases rapidly. This creates energy with which particles can be created. Where you might expect two unbounded quarks, hadrons are formed instead. They can be grouped into mesons consisting of a quark and antiquark or baryons consisting of three quarks. Colour confinement thus explains why we do not observe quarks or gluons flying around by themselves.

2.3 Quark Gluon Plasma

In short, the Quark Gluon Plasma is the "deconfined state of strongly interacting matter" [8]. What does this mean? We take a look at a nucleus containing some hadrons. As a result of confinement, these stay together. However, at high densities, the hadrons start overlapping. This causes the constituents to be unable to recognize who it used to be bounded to, thus resulting in a pool of unbounded quarks. Similarly, at high temperatures the hadrons decay into a lot of lower mass hadrons, usually pions. As the density increases, the quarks find themselves free of their former partner quarks. This is what we know to be a quark gluon plasma. The temperature for which the matter transitions into a QGP is called the critical temperature and is approximately 156 MeV as can be seen in 2.3.

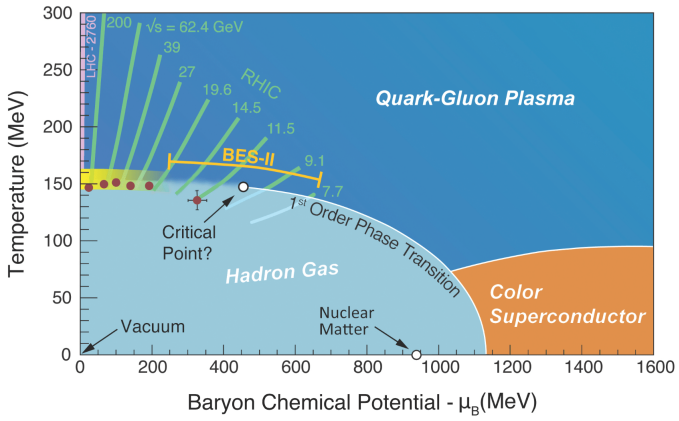

Figure 2.3: Phase diagram of QCD matter. This diagram shows the critial temperature where matter transitions into Quark Gluon Plasma. [28]

2.4 Suppression and regeneration in QGP

Mesons made of heavy quarks, such as the bottom and charm quark, were suggested as probes already in 1986 when Matsui and Satz suggested to use the J/ψ meson to probe the QGP [8]. As mentioned in the introduction, heavy quark mesons are mostly created in the initial hard collision before the matter transitions into a QGP. They thus go through the whole evolution of the QGP showing their potential as "particle thermometers".

During their journey through the QGP, they experience quark colour screening. Consequently, the production of quarkonium states with low bonding energy can result in suppression throughout the full evolution of the QGP. Where the temperature increases, the binding radius of the heavy quark meson eventually becomes smaller than the colour screening radius resulting in the melting of the composite particle. There are multiple factors influencing the suppression. For example, the smaller the radius of the hadron, the tighter bound it is and the later it melts in the QGP. There are even differences in melting for the different bound states of a particular composite particle. Suppression can thus be used to reconstruct the temperature of the QGP.

Furthermore, there is a process called regeneration or recombination. If free flying quarks get close enough to each other in phase space, they can (re)combine into a heavy quark meson. This process happens next to suppression and complicates the investigation of the temperature.

In the introduction the use of the J/ψ ($c\bar{c}$) and Υ ($b\bar{b}$) mesons as probes were mentioned. Both are quarkoniums meaning the meson states are bounded by a heavy quark and its anti-quark. As the charm quark is lighter than the bottom quark and therefore more abundantly produced in high energy collisions, the quarkoniums made of charm quarks and antiparticle were used earlier than its brother.

Already in 1997 in the NA50 experiments at SPS, high-statistics data was available on the suppression of the J/ψ meson proposing its potential as a probe through the QGP [3]. However there were other factors non-related to the Quark Gluon Plasma that influenced the suppression of these mesons, which interfered with its potential as a probe.

The Υ showed to be a useful "particle thermometer" for the first time at the CMS experiment at the LHC in 2011 [4]. Compared to J/ψ mesons, Υ lepton pair decays are more cleanly detected. Furthermore, the CMS detector has an outstanding dilepton mass resolution [4]. While earlier the distinction between the three mass peaks with the lowest-energy Upsilon state (Υ(1S)) and its first two excited states (Υ(2S) and (Υ(3S)) had only been observed in proton-antiproton collisions at the Tevatron [18], CMS managed to cleanly differentiate the peaks in heavy ion collisions. They found that at higher temperatures the higher upsilon states were more suppressed relatively to the ground upsilon state and relatively to the production in pp collisions. Such sequential suppression (with upsilon(3S) almost fully melted in Pb-Pb collisions) can be related to the temperature of the plasma once considered the different Debye length of the three states.

However, ALICE and CMS analyze heavy-ion data from the large hadron collider, at a center of mass energy of $\sqrt{s_{NN}} = 5.02$ TeV which is far higher than the one previously available. Therefore, when using the J/ψ or the Υ mesons to probe the Quark Gluon Plasma, regeneration needs to be taken into account. Using D mesons as temperature probes is what is suggested for the first time in this thesis. They differ from earlier mesons used as they only have one charm quark and another different anti-quark. This means they will have different Debye lengths and therefore different melting points and different regeneration rates. Consequently, the use of the D mesons can give a different perspective on the measurement of the temperature, adding information and allowing to better constrain the role of regeneration.

2.5 Higher D^* meson states

D mesons are part of the open heavy-flavoured mesons meaning that one of the valence quarks is a heavy-quark. In the case of D mesons this is the charm quark and D mesons are actually the lightest particles comprised of this quark flavour. In this study, we are particularly interested in $D^*(2010)^+$, $D_0^*(2400)^0$, $D_1(2420)^0$ and $D_2^*(2460)^0$. The configuration of the particles is as follows: $D^*(2010)^+$ is a meson made up of a charm and a down quark and the other D meson states are comprised of a charm and an up quark. There are two ways in which D mesons can be produced. There is the more straight forward way where the D meson is created immediately through the hadronisation of a charm quark. This process is called prompt. The other way of producing a D meson is through the decay of a B meson. This is called feed-down. B mesons are also open heavy-flavoured mesons. Contrarily to D mesons, B mesons contain the bottom quark as one the valence quarks and are thus heavier.

There are three decay modes for $D^*(2010)^+$. In order to choose the decay for which $D^*(2010)^+$ is easiest reconstructed, we have to take multiple factors into account. First the branching ratio is an important factor, the higher the branching ratio, the more probable is that the D meson will decay in the channel of interest and therefore, the chance to reconstruct it starting from the decay products is higher. This is not the only important factor, one has to think about whether the daughters are well detected and if they are distinguishable from the background. For $D^*(2010)^+$ the best decay is given by

$$D^*(2010)^+ \to D^0 \quad \pi^+ \qquad\qquad D^0 \to K^+ \quad \pi^-$$

with a branching ratio of 67.7 ($\pm$ 0.5)%. The same reasoning is applied to the other mesons. For these the following decays were chosen:

$$D_0^*(2400)^0 \to D^+ \quad \pi^- \qquad\qquad D^+ \to K^0 \quad \pi^+$$

$$D_1(2420)^0 \to D^*(2010)^+ \quad \pi^- \qquad D^*(2010)^+ \to D^0 \quad \pi^+ \qquad D^0 \to K^+ \quad \pi^-$$

$$D_2^*(2460)^0 \to D^+ \quad \pi^- \qquad\qquad D^+ \to K^0 \quad \pi^+$$

As compared to $D^*(2010)^+$, not much is known about the decays of $D_0^*(2400)^0$, $D_1(2420)^0$ and $D_2^*(2460)^0$. Some of their decays are merely theoretical or unseen and the chosen decays as seen above have been observed, but their branching ratio is unknown.

Chapter 3

Large Hadron Collider

The particle accelerator that CERN uses to test the Standard Model and the phenomena it predicts, is the Large Hadron Collider (LHC). The particle accelerator was first run in 2008 and with its 27-kilometer ring of superconducting magnets is the most powerful particle accelerator ever built [13]. The LHC is the last of a succession of machines in which the energies of the accelerated particles is boosted. Over those 27 kilometers a particle's energy reaches its highest values for a speed that is about 0.9998 the speed of light. They are navigated through the pipes by a strong magnetic field brought about by superconducting electromagnets. Collisions of the particles happen in four locations around the LHC and correspond to the four different detectors: ATLAS [1], CMS [10], ALICE [20] and LHCb [11].

3.1 ALICE detector

ALICE focuses on heavy-ion collisions with the purpose to further investigate the theory behind the strong force. In figure 3.1 the setup of the detector can be seen. In the central barrel one can find the Inner Tracking System (ITS) and the Time-Projection Chamber important for particle detection and identification.

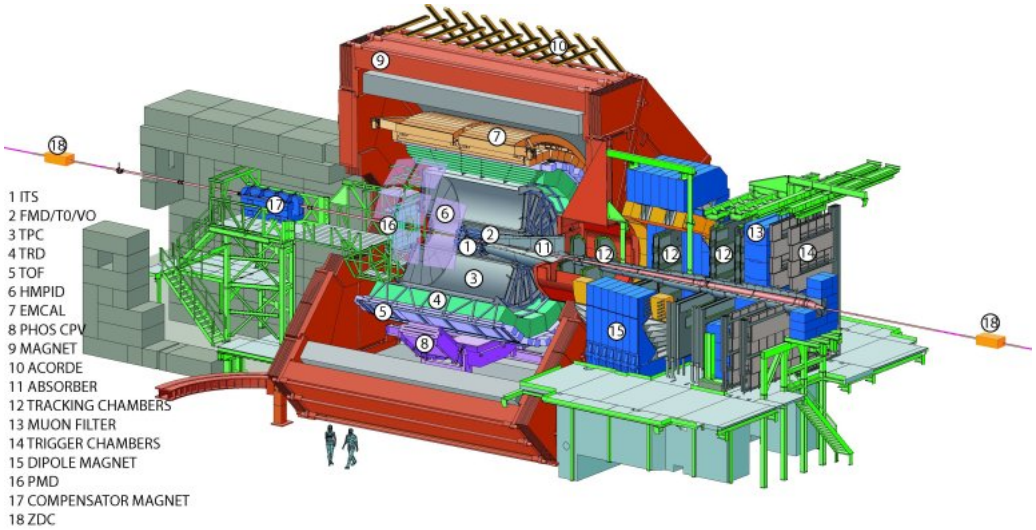

Figure 3.1: The ALICE detector setup showing the 18 detectors of the experiment [**alicedetector**].

3.1.1 Inner Tracking System

The Inner Tracking System's main purpose is to determine the location of the primary and secondary vertices from charmed meson and hyperon decays with an accuracy of a few tens of micrometers [20]. Secondly, it aims to track and identify low-momentum particles. This is important, because they are not detected by the Time Projection Chamber. Lastly, the ITS' objective is to enhance the momentum resolution for high-momentum particles. For the third LHC run, which will commence in 2021, an upgraded ITS will be used [26]. In this subsection I will first explain how the previous ITS worked and will continue by discussing the improved ITS.

The previous ITS' system is made up of six cylindrical layers of silicon detectors which surround the beam pipe at the position of collision. The rapidity range of the detector is limited to $|\eta| \leq 0.9$ and stretches in all directions around the beam pipe as far as the interaction diamond goes, 10.6 cm [20]. There are some factors that influence the radii of the cylindrical layers. One requirement is that the tracks of the ITS match those of the TPC. Furthermore, the inner radius is determined by the clearance between the ITS and the beam pipe. In order to record the lower momentum particles, the thickness of the material also had to be minimized as much as possible. With this in mind, all layers are made of light-weight construction material and most electrical connections use aluminium

on polyimide cables.

For the silicon sensors, three different technologies were used. The two most inner layers are made up of silicon pixel detectors (SPD). The two middle layers are made up of silicon drift detectors (SDD) and the outer two are made up of silicon strip detectors (SSD). The SPD's purpose is to pick out the secondary vertices of charm and beauty quarks in such a high multiplicity environment. These two inner layers have a pseudorapidity range of $|\eta| < 1.98$ unlike the other layers [25]. These help accomplish a track impact parameter resolution in the plane perpendicular to the beam axis above 50 μm for $p_t > 1.3$ GeV/c [22]. The two middle layers consist of SDD. After a particle passes the SDD, electrons are liberated. Because of an applied electric field, the electrons drift towards channels. The y and x coordinate of the particle can be measured through this method. The outer two layers use SSD. This is connected to the external detectors such as the TPC and thus contribute to the connected tracking of the particles. Next to that, the SSD measures the particle's energy loss which helps to identify the particle.

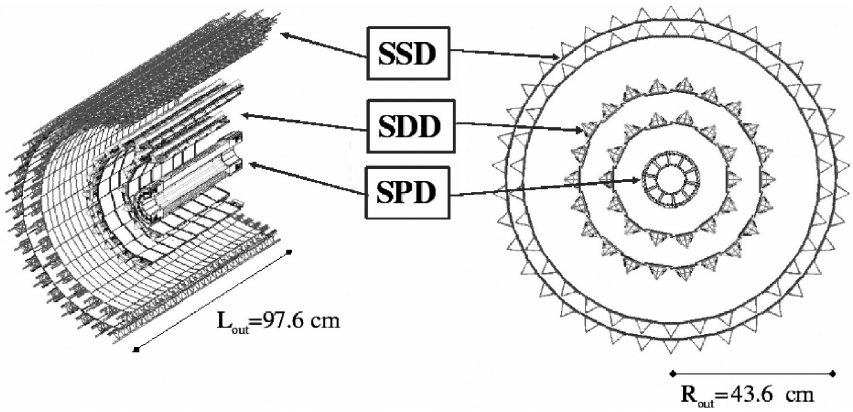

Figure 3.2: Both a cut-away and sliced view of the ITS show the silicon layers of the ITS [20].

The upgraded Inner Tracking System contains seven layers of a CMOS Monolithic Active Pixel Sensor (MAPS) design known as ALice PIxel DEtector (ALPIDE). The seven layers can be regarded as built up of three inner layers called the Inner Barrel (IB) and the outer four layers, the Outer Barrel (OB). The OB can be further split into two inner layers (IL) and two outer layers (OL). The three IB layers have a varying amount of IB staves. Each stave consists of a cold plate, a space frame and an IB module which contains 9 ALPIDE chips. The four OB layers consist of two half staves that overlap. In the OL each half stave contains 7 OB modules, whereas the IL each has 4 OB modules. These OB modules

have 14 ALPIDE chips organized into two parallel rows of 7.

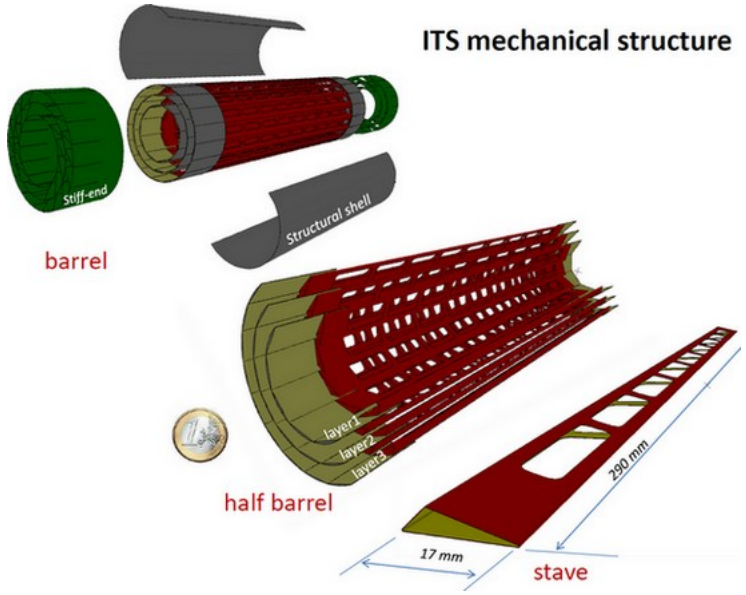

Figure 3.3: The construction of the upgraded Inner Tracking System (ITS) is shown in a schematic way [16].

Comparison upgraded ITS with its predecessor

The new ITS' readout rate has been improved to 100 kHz, which is twice the interaction rate for a Pb-Pb collision [17]. Furthermore the radius of the first layer of the ITS decreased from 39 mm to 23 mm. Where the previous tracker covered a speudorapidity region of $|\eta| < 0.9$, the improved tracker can cover $|\eta| < 1.22$ for the 90% most luminous area. The tracker has an active region of approximately 10 m^2, divided into 12.5 billion pixels. As a consequence of these improvements, the impact parameter resolution has bettered with a factor six in the direction along the beam axis (from 240 μm to 40 μm) and with a factor three in the transverse plane (from 120 μm to 40 μm) at a transverse momentum of 500 MeV/c.

3.1.2 Time Projection Chamber

The Time Projection Chamber (TPC) is the main tracking device of ALICE [14]. The advantages of this type of detector are its ability to capture all the information of tens of thousands of particles produced in the collision in the accepted pseudo-rapidity range. These outshine its lack of recording speed and huge data volume.

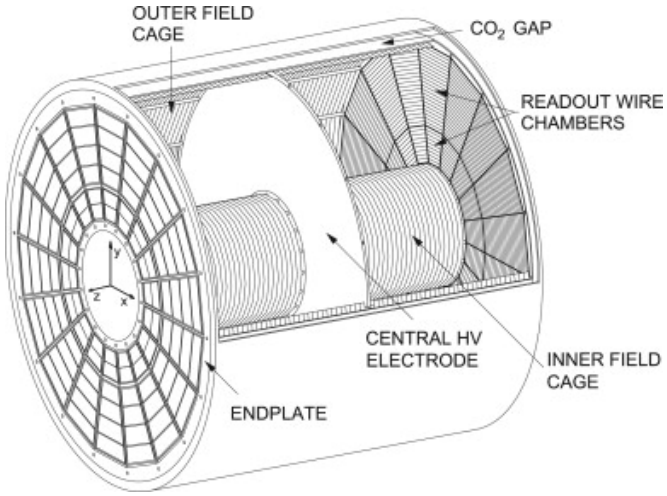

Figure 3.4: Schematic of ALICE's Time Projection Chamber (TPC) [21].

The setup of the TPC can be seen in figure 3.4. The charged particles come into the TPC and leave ionizing tracks in the gas that fills the cylinder. This cylinder is split into two halves by the central electrode. Because of the strong electric field of 100 kV, the ionized electrons slowly start moving towards the two ends of the TPC. Here, they are amplified and recorded in wire chambers. The signal recorded in both end chambers give us their two coordinates of arrival. The drift time allows us to calculate the distance of the track from the end plate, which enables us to thoroughly distinguish the tracks of the many particles of the collision.

The materials and gas chosen for the detector ensure that the ALICE detector is a remarkably low mass detector. The field cage which is 5.6 meters in diameter and 5.4 meters long is made up of two Carbon-fiber/honeycomb composite cylinders, which space-applications are also made of. Another factor that influences its performance are the dimensional tolerances, which therefore were kept at the 10^{-4} level. The central electrode responsible for the drift of the electrons was built with planarity and parallelism to the readout chambers of better than 0.2 mm. Next to these, Neon was chosen as the chamber gas, which is lighter than the usual Argon gas thus contributing to a low-mass TPC. However, Neon gas' environmental conditions have to monitored as pressure and temperature have a strong dependence on drift velocity. Therefore, the temperature has to have a stability of approximately $0.1C^{\circ}$ over the volume of 90 m^3, which was employed at the detector.

As for the readout electronics, they are given by a preamplifier/ signal shaper which

functions at the fundamental thermal limit of noise and a specially developed readout chip named the ALICE Tpc Read Out (ALTRO) chip. These are responsible for processing the signals digitally which is ideal its performance at high collision rates. The electronics are fully stationed on the end plates of the TPC and are connected to the Data Acquisition System by just 260 optical fibers.

3.1.3 Time of Flight

The Time-of-Flight System (TOF) is important in the particle identification process [14]. The flight time of the particles after collision together with their momentum can determine their mass and thus enables us to differentiate between pions, kaons and protons up to a few GeV/c.

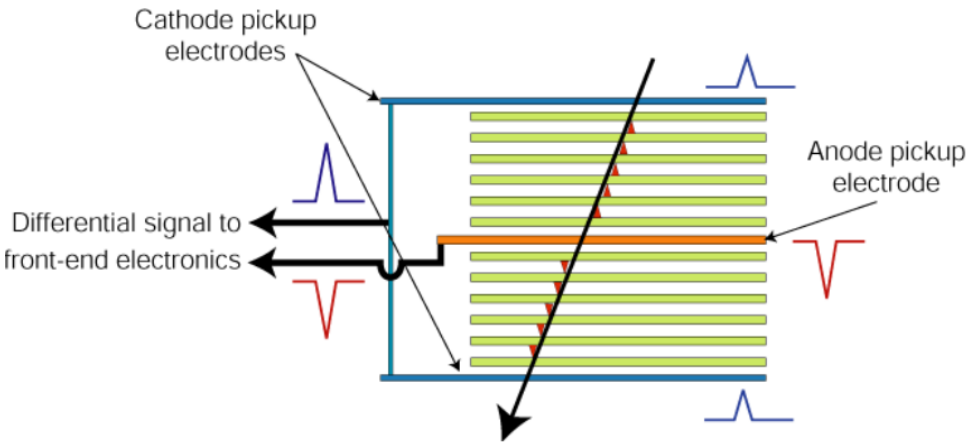

Figure 3.5: Schematic of the Multigap Resistive Plate Chamber (MRPC) which is a part of the Time-of-Flight (TOF) detector [6].

The Multigap Resistive Plate Chamber (MRPC) is the detector with which $5\text{x}10^{-11}$s (50 ps) time resolution is reached [14]. This is a necessity in the presence of the extreme particle multiplicities. It consists of numerous resistive glass plates. On the outside of the glass plates a high voltage is applied. When a charged particle passes, it ionises the gas which is amplified by the electric field. The liberated electrons give off a signal to pickup electrodes situated outside of the glass plates. The total signal is then the sum of the signals form all the gaps.

Chapter 4

Methodology

The goal of this study is to see if it possible to reconstruct $D_0^*(2400)^0$, $D_1(2420)^0$ and $D_2^*(2460)^0$ with $D^*(2010)^+$ in pp collisions at $\sqrt{s} = 13$ TeV in order to see if it is possible to set a reference for Pb-Pb studies and to see if it is feasible to consider these D mesons as probes for the QGP. It is first important to see the quantities in which the specific D mesons are produced. If not enough D mesons are produced or if they suggest to be a problem to reconstruct, then we can conclude that these mesons are not worth looking into during the third run of ALICE. Nevertheless, if it turns out that they are promising probes, we would want to study the kinematic properties of these mesons in simulations in order to gain experience and prepare a reconstruction strategy on real LHC data.

4.1 Simulations

In order to study the kinematic properties of $D_0^*(2400)^0$, $D_1(2420)^0$ and $D_2^*(2460)^0$ and $D^*(2010)^+$ in p-p collisions, we use state-of-art computer simulations. In this study we used the framework ROOT version 6 [7] and configured this with PYTHIA8 [24]. In the sections below the programs ROOT and PYTHIA will be explained in more detail. Furthermore, I will explain some aspects of the code that selected the specific decays of $D_0^*(2400)^0$, $D_1(2420)^0$, $D_2^*(2460)^0$ and $D^*(2010)^+$ discussed in section 2.5 and the properties that were looked into.

4.1.1 ROOT framework

ROOT is a framework developed by CERN itself and thus perfectly suits particle physics projects [7]. The framework is used for data processing and is written in C++. It has

many applications such as saving data in a compressed binary form in a ROOT file. It also offers a convenient data structure to save and organize large amounts of data. This structure is called a tree. ROOT has the ability to mine data too. This means to say that ROOT enables you to use their mathematical and statistical tools. Any kind of data manipulation is possible and it can simulate complex systems. It can publish results, meaning results can be presented in histograms, scatter plots et cetera.

4.1.2 PYTHIA

PYTHIA is a program that was developed for generating high-energy particle collision events [24]. It presents users with a set of models that brings a hard-scattering process to a multiparticle final state. Previous versions of PYTHIA used the programming language fortan. However, the newer version, PYTHIA8, uses C++ and is the version used in this study.

In PYTHIA there are multiple scattering processes that can be simulated. In our case we look at QCD-processes. These can be split into hard-QCD processes and soft-QCD processes. The first means that there is open charm and bottom production. The consequences are that there are more charm and bottom quarks around which results in larger amounts of D mesons produced in the simulations. On the contrary, soft-QCD processes are minimum-bias collisions and therefore more similar to natural collisions. In this project the collisions simulated were a soft scattering process using the code

$$\text{pythia8} \rightarrow \text{ReadString}(\text{"SoftQCD:all = on"});$$

Additionally, it is possible in PYTHIA to modify certain decay channels to be on or off and adjust the branching ratio. In the code in this project the code below was used. All D^+ mesons were forced to decay into K^0 and π^+. This implies that the branching ratio for this decay becomes 100%.

$$\text{pythia8} \rightarrow \text{ReadString}(\text{"411:onMode = off"});$$

$$\text{pythia8} \rightarrow \text{ReadString}(\text{"411:onIfMatch = 311 211"});$$

The same was done for all D^0 mesons. They were forced to decay into K^+ and π^+. Again the branching ratio for this decay becomes 100%.

$$\text{pythia8} \rightarrow \text{ReadString}(\text{"421:onMode = off"});$$

pythia8 $\rightarrow$ ReadString("421:onIfMatch = 321 211");

Furthermore, the meson $D_1(2420)^0$ only allowed decay channels were $D^*(2010)^+$ was produced and similarly for meson $D_2^*(2460)^0$ decays where D^+ was produced were turned on.

pythia8 $\rightarrow$ ReadString("10423:onMode = off");

pythia8 $\rightarrow$ ReadString("10423:onIfAny = 413");

pythia8 $\rightarrow$ ReadString("425:onMode = off");

pythia8 $\rightarrow$ ReadString("425:onIfAny = 411");

These decay modes were altered with the purpose of enhancing the production of $D_0^*(2400)^0$, $D_1(2420)^0$ and $D_2^*(2460)^0$ in each event. This was necessary as these specific D meson states are relatively rare and consequently a large amount of events have to be generated in order to get the required amount of statistics to research them.

4.1.3 Analysis

In this study, proton proton collisions were simulated at an energy of 13 TeV. The kinematic properties of all four D meson states, all their daughters and all the charged particles, which are mostly pions, had to be saved. In order to efficiently save this large amount of data, the information was put into a tree and divided into branches and leafs. The kinematic properties that were saved for the D mesons and charged particles were amount of the particle produced, the p_t, η, ϕ and V_x, V_y, V_z, while for the daughters only the the p_t, η and ϕ were saved. Each D meson was given their own branch containing their own kinematics and those of their daughters. The charged particles and all particles together also had their own branches. During each generated event, all particles were looped to see if its PDG matched with one of the D mesons and whether their daughters matched the chosen decays of $D_0^*(2400)^0$, $D_1(2420)^0$, $D_2^*(2460)^0$ and $D^*(2010)^+$. If they did match, then all leafs were filled.

Quantity of the D mesons

One of the important first steps for this research is to establish in which amounts $D_0^*(2400)^0$, $D_1(2420)^0$, $D_2^*(2460)^0$ and $D^*(2010)^+$ can be expected in the third run of ALICE. In the previous two runs, about 2 billion events could be recorded [12]. With

ALICE's upgraded detector about ten times as many statistics can be recorded [2]. This is then also the amount that we want to give an expected number for using the simulations.

Because the decay of D^+ and D^0 were forced to 100% and the decays of $D_1(2420)^0$, $D_2^*(2460)^0$ were adjusted in some way, we need to take this into account when calculating the number of D mesons expected per event and for the expected 20 billion of statistics. Below, all selected decays can be seen. If the specific decay is underlined, it is a forced decay.

$$D^*(2010)^+ \to D^0 \quad \pi^+ \qquad \underline{D^0 \to K^+ \quad \pi^-}$$

$$D_0^*(2400)^0 \to D^+ \quad \pi^- \qquad \underline{D^+ \to K^0 \quad \pi^+}$$

$$\underline{D_1(2420)^0 \to D^*(2010)^+ \quad \pi^-} \qquad D^*(2010)^+ \to D^0 \quad \pi^+ \qquad \underline{D^0 \to K^+ \quad \pi^-}$$

$$\underline{D_2^*(2460)^0 \to D^+ \quad \pi^-} \qquad \underline{D^+ \to K^0 \quad \pi^+}$$

The accurate amount of $D_0^*(2400)^0$, $D_1(2420)^0$, $D_2^*(2460)^0$ and $D^*(2010)^+$ per event can be recalculated by using the observed branching ratio from the PDG. We know the branching ratio for $D^0 \to K^+ \quad \pi^-$ is given by 3.950%. Therefore we can calculate the right number of $D^*(2010)^+$ per event

$$\#D^*(2010)^+ \text{ per event } = \#D^*(2010)^+ \text{ measured } \cdot 0.03950 \; / \# \text{ events}$$

However, we come across a problem when we try to use the same method for the other D mesons. In the PDG, the branching ratio for $D_0^*(2400)^0$, $D_1(2420)^0$, $D_2^*(2460)^0$ decays are unknown. Another method would be to look at the decays that the PDG has seen for each of the mesons and calculate their branching ratio that way. However, this turned out to be rather complicated seeing that PYTHIA also put in additional theoretical decays for the mesons not shown in the PDG, such as $D_2^*(2460)^0 \to D^*(2007)^0 \quad \pi^0$. This problem was solved by taking the ratio with $D^*(2010)^+$ and thus still finding the right numbers for the other D mesons.

Chapter 5

Results

Simulations of 10 million pp collisions were executed at a center of mass energy of 13 TeV using ROOT and PYTHIA. In table 5.1 the number of higher D^* meson states as measured in the simulated 10 million events is shown. The actual ALICE detector, however, is not free of faults and its performance cannot said to be equivalent to that of the computer simulations. As explained in chapter 3, the pseudo-rapidity range of the ITS detector is limited to $|\eta| < 0.9$, the D meson states that will be recorded during the third run will be within this limit and are thus recorded in lesser quantities as compared to the simulations. Another factor that needs to be taken into account is the upgrade of ALICE's detector which will result in an increase in recorded collisions. For the third run, it is predicted that $\sim$ 20 billion collisions can be recorded [12] [2]. Therefore the final results were scaled to 20 billion collisions. In table 5.1 the quantities of $D^*(2010)^+$, $D_0^*(2400)^0$, $D_1(2420)^0$ and $D_2^*(2460)^0$ ALICE can expect in the third run in 2021 in 20 billion collisions both with and without a $|\eta| < 0.9$ cut can be seen.

D meson state	$D^*(2010)^+$	$D_0^*(2400)^0$	$D_1(2420)^0$	$D_2^*(2460)^0$
Number in 10 million events without η cut	273886	524	756	1368
Number per event without η cut	$1.082 \cdot 10^{-3}$	$2.070 \cdot 10^{-6}$	$2.986 \cdot 10^{-6}$	$5.404 \cdot 10^{-6}$
Number per 20 billion events without η cut	$2.164 \cdot 10^{10}$	$4.140 \cdot 10^{7}$	$5.972 \cdot 10^{7}$	$1.081 \cdot 10^{8}$
Number in 10 million events with η cut	69428	92	188	298
Number per event with η cut	$2.742 \cdot 10^{-4}$	$3.634 \cdot 10^{-7}$	$7.426 \cdot 10^{-7}$	$1.177 \cdot 10^{-6}$
Number per 20 billion events with η cut	$5.485 \cdot 10^{9}$	$7.268 \cdot 10^{6}$	$1.485 \cdot 10^{7}$	$2.354 \cdot 10^{7}$

Table 5.1: The quantities that were simulated and that can be expected in ALICE's third run for $D^*(2010)^+$, $D_0^*(2400)^0$, $D_1(2420)^0$ and $D_2^*(2460)^0$.

In ALICE detectors it is not the D mesons, but their daughters that are detected. In order to investigate $D_0^*(2400)^0$, $D_1(2420)^0$ and $D_2^*(2460)^0$ it is useful to find ways to distinguish between the daughters of the higher D^* meson states and the other charged particles, which are mostly pions and will be called background in the rest of the thesis. In figure 5.1 ratio plots of the p_T of the higher D^* meson states divided by $D^*(2010)^+$ are presented. Because the magnitude of occurrence of the D meson states differs (see table 5.1), each had to be normalized and scaled in order to compare the shapes of the p_T distributions. We can see that the ratio between a higher D^* meson and $D^*(2010)^+$ for lower p_T is close to 1. This implies that their p_T distributions have a similar shape in the low/intermediate p_T range. At higher p_T, the p_T distributions of $D_0^*(2400)^0$, $D_1(2420)^0$ and $D_2^*(2460)^0$ seem to have a softer shape than $D^*(2010)^+$. This implies that at higher p_T it will be more difficult to distinguish between $D_0^*(2400)^0$, $D_1(2420)^0$ and $D_2^*(2460)^0$ for their peaks are broader.

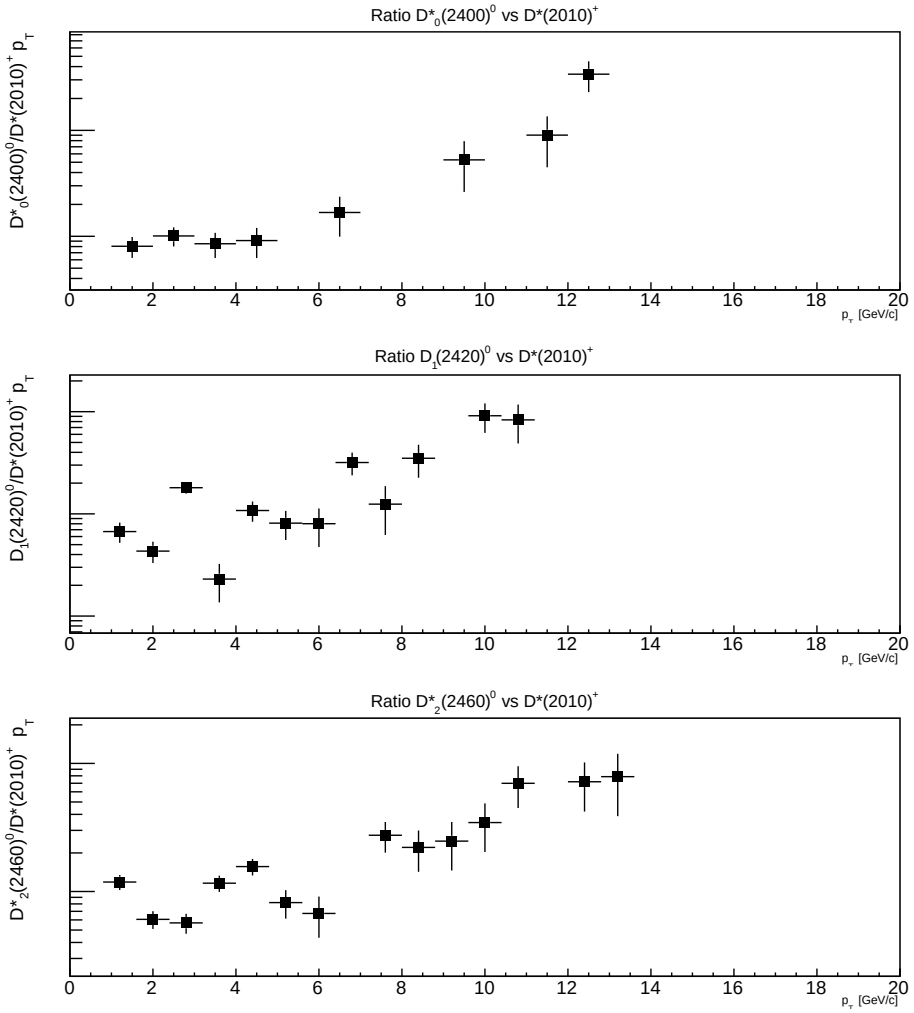

Figure 5.1: Plots show the ratio between the p_T of $D^*(2010)^+$ and $D_0^*(2400)^0$, $D_1(2420)^0$ and $D_2^*(2460)^0$.

The production vertexes of all charged particles, $D^*(2010)^+$, $D_0^*(2400)$, $D_1(2420)^0$ and $D_2^*(2460)^0$ can be seen in figure 5.2. Interestingly, the mean coordinates of the production vertex of the charged particles are close to the primary vertex which is (0,0) by convention since most of the particles are created at the collision point. Contrarily, the mean coordinates of the production vertexes of $D^*(2010)^+$, $D^*(2010)^+$, $D_0^*(2400)$ and $D_1(2420)^0$ have values larger by a factor $\sim 10^3$. Even within the D mesons a difference in values can be seen. The production vertex of $D^*(2010)^+$ is localized almost stably at $(-0.001328, 0.0006691)$, whereas the other mesons have larger values with a factor between 10^1 and 10^2 and deviate from the mean more. In figure 5.3, the mean decay length of $D^*(2010)^+$, $D^*(2010)^+$, $D_0^*(2400)$ and $D_1(2420)^0$ is shown. It supports the previous

observation of further outlying production vertex coordinates for the higher D^* meson states as compared to $D^*(2010)^+$.

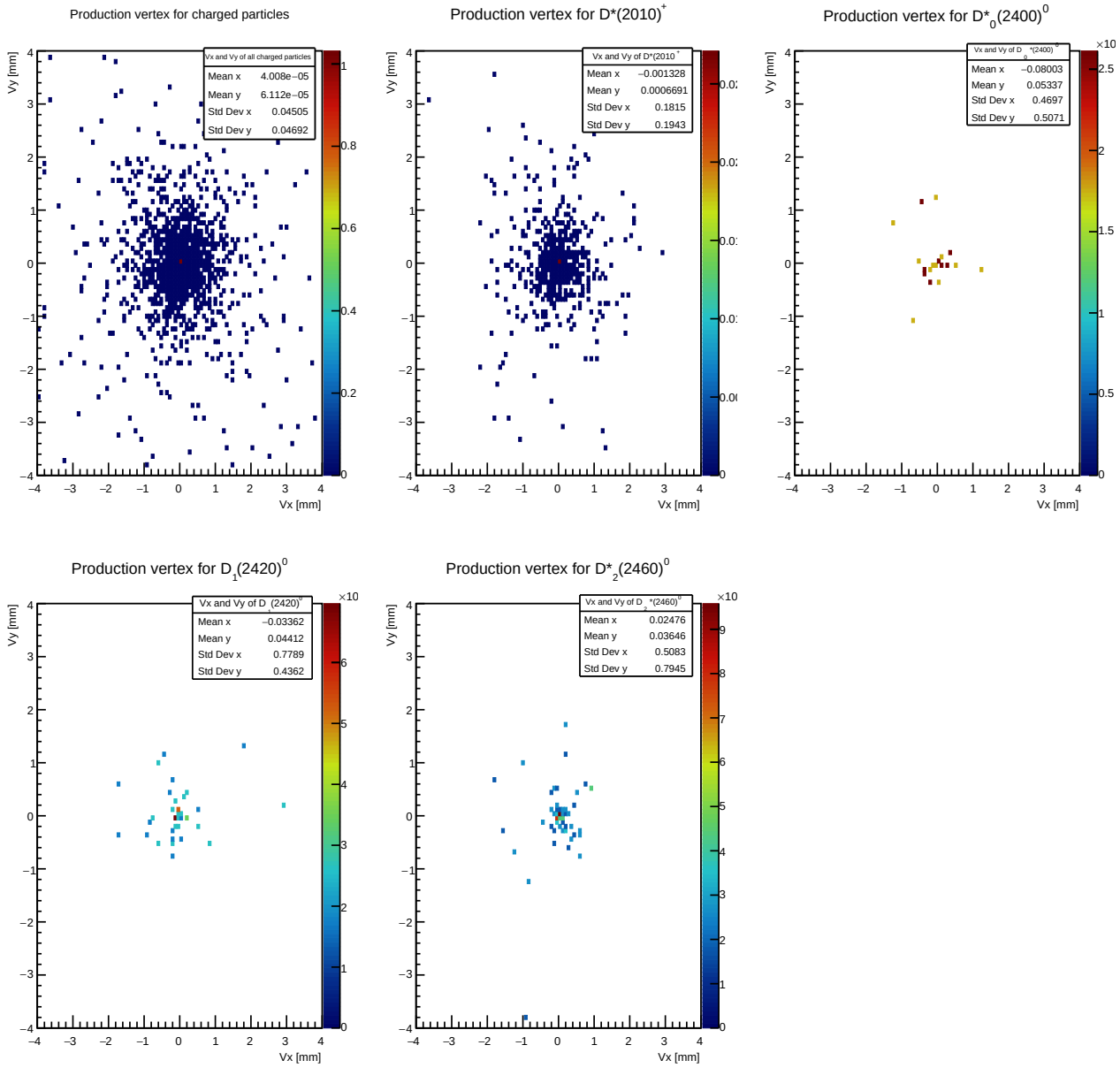

Figure 5.2: Production vertexes of $D^*(2010)^+$, $D_0^*(2400)$, $D_1(2420)^0$ and $D_2^*(2460)^0$. These show the mean decay lengths of these mesons as compared to the initial collision point. Blue shows little entries, while red and yellow show a higher percentage of the mesons.

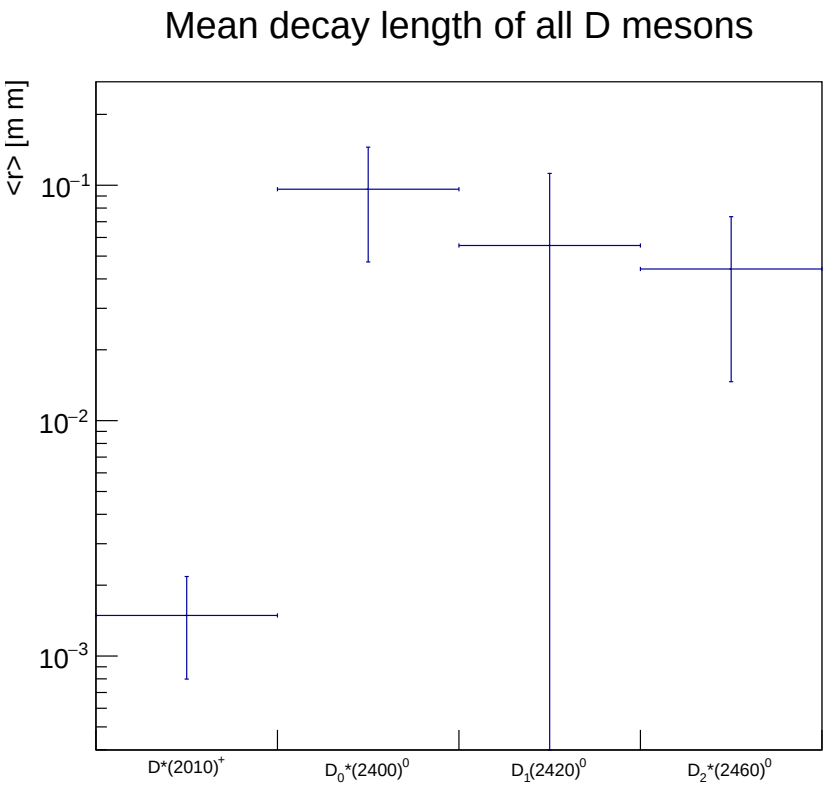

Figure 5.3: Mean decay length of $D^*(2010)^+$, $D_0^*(2400)$, $D_1(2420)^0$ and $D_2^*(2460)^0$, given by $< r >= \sqrt{V_x^2 + V_y^2}$.

One of the daughter particles of $D^*(2010)^+$, $D_0^*(2400)$, $D_1(2420)^0$ and $D_2^*(2460)^0$ is the soft pion which are pions with low momentum values. Their efficient detection is necessary to reconstruct the mother particle. It is thus useful to look at the soft pions of $D^*(2010)^+$, $D_0^*(2400)$, $D_1(2420)^0$ and $D_2^*(2460)^0$ to see if their kinematic properties enable us to separate them from the background. In figure 5.4 the correlation between the p_T of each individual meson and its soft pion can be seen. If there is a correlation, one can look what the relation is between the two particles and based on this cut out part of the background. Where there seems to be a correlation for $D^*(2010)^+$ between the momentum of $D^*(2010)^+$ and its soft pion, there does not seem to be such a correlation for the other mesons. Correlation between the p_T of the higher D^* meson states and their soft pion can thus not be used to better reconstruct the D mesons.

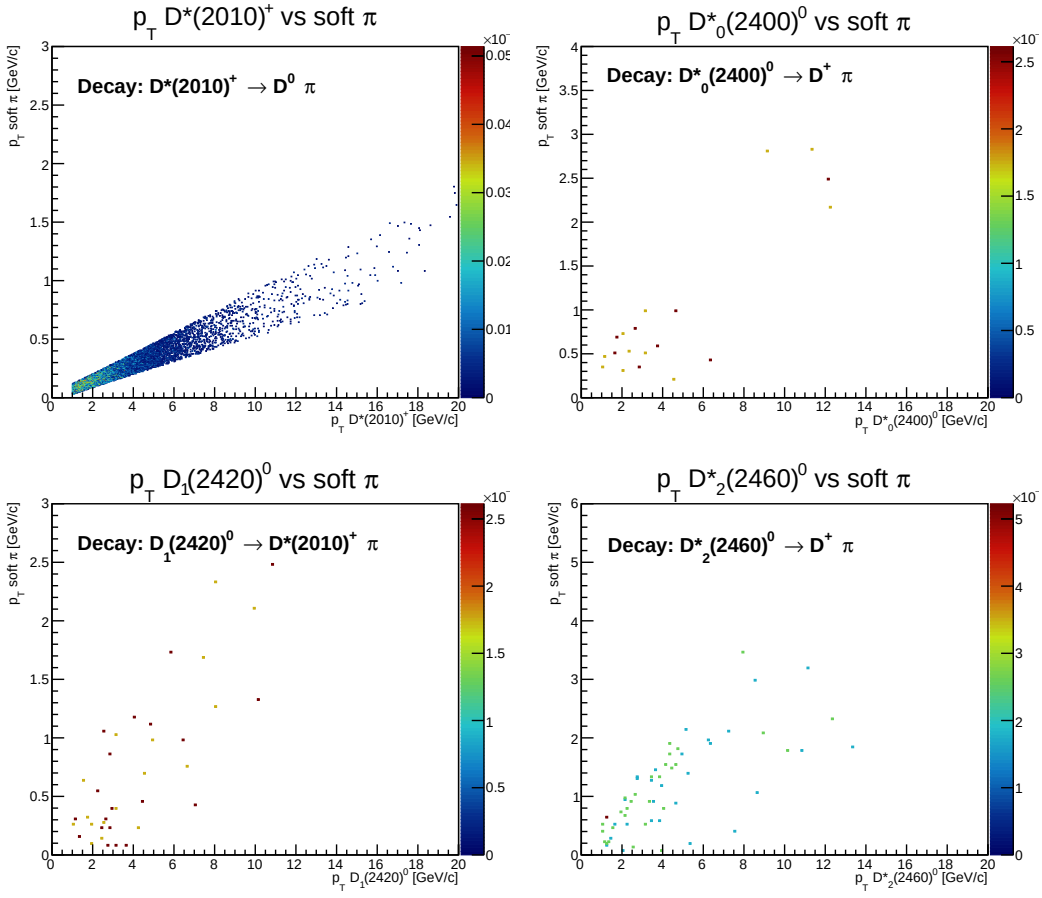

Figure 5.4: Correlation of each individual meson with its soft pion. Dark blue means that there is a low number of entries, where red indicates a high number of entries.

Another way of differentiating the soft pions from the background is by looking at their p_T distributions. In figures 5.7, 5.8, 5.9, 5.10 the p_T of the D mesons is divided into bins ranging from [0,1 GeV/c] to [8-9 GeV/c]. The p_T of the corresponding soft pion is plotted against the p_T of the inclusive pions for each bin. In figure 5.5a, 5.5b, 5.6a, 5.6b one can clearly see the peak of soft pion p_T migrate from low to higher values as the p_T of the bins increases.

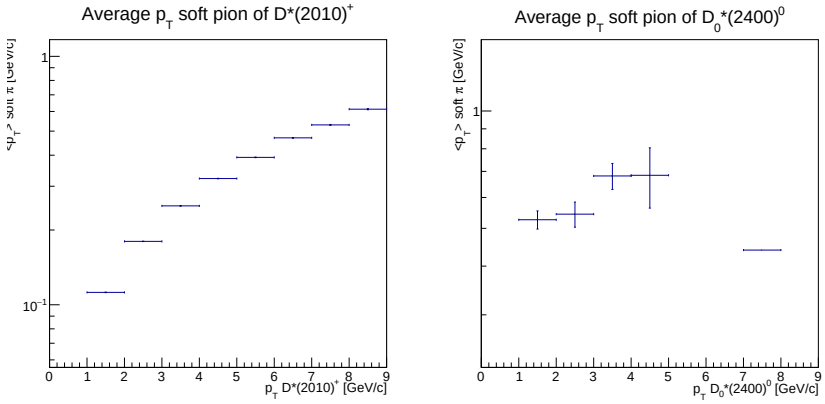

(a) Average p_T of the soft pion as a function of $D^*(2010)^+$

(b) Average p_T of the soft pion as a function of $D_0^*(2400)^0$

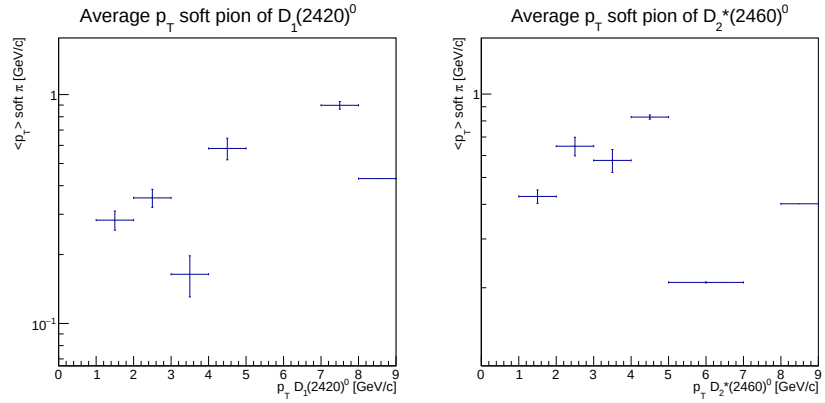

(a) Average p_T of the soft pion as a function of $D_1(2420)^0$

(b) Average p_T of the soft pion as a function of $D_2^*(2460)^0$

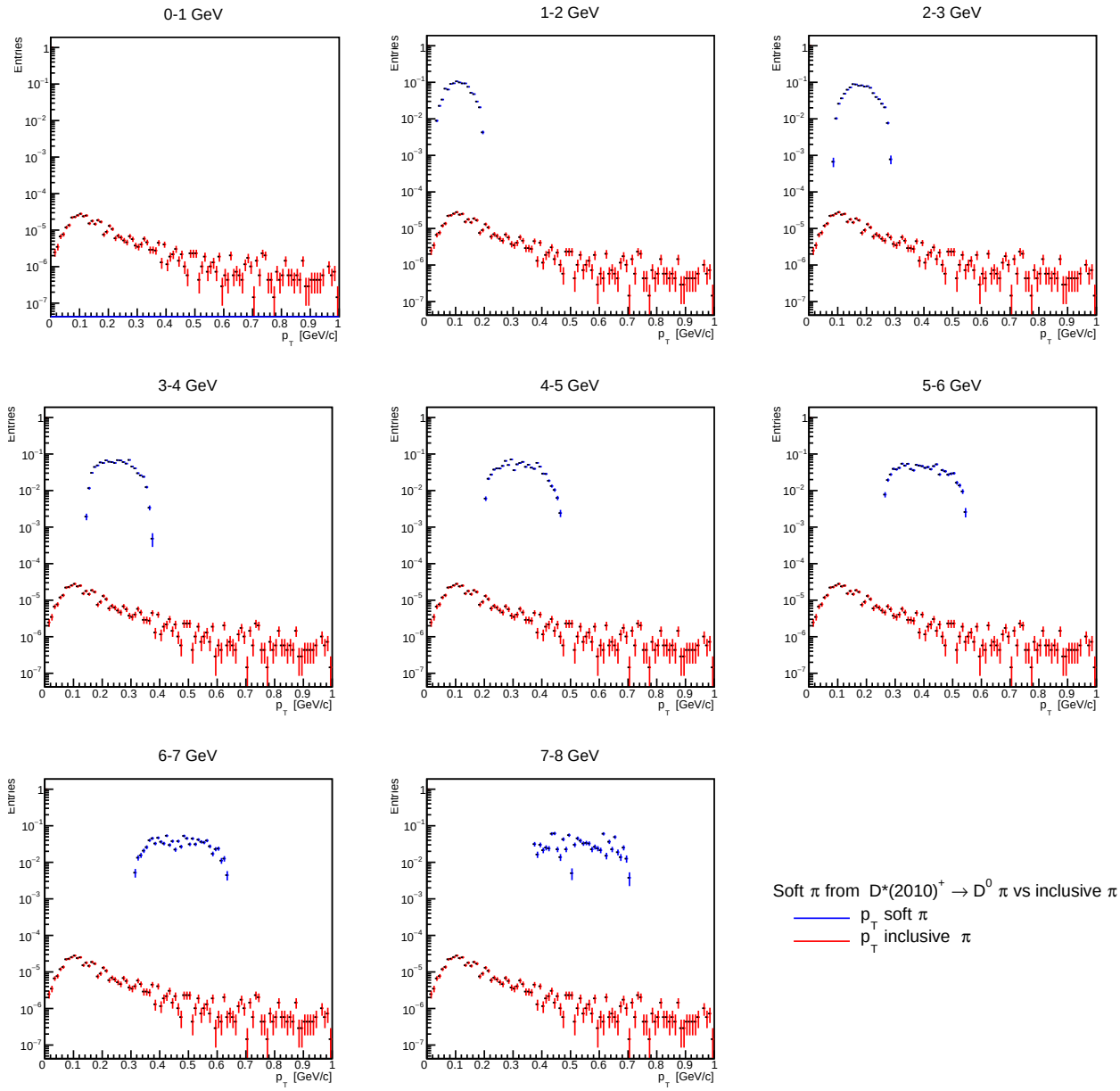

Figure 5.7: Soft pions $D^*(2010)^+$ versus inclusive pions p_T

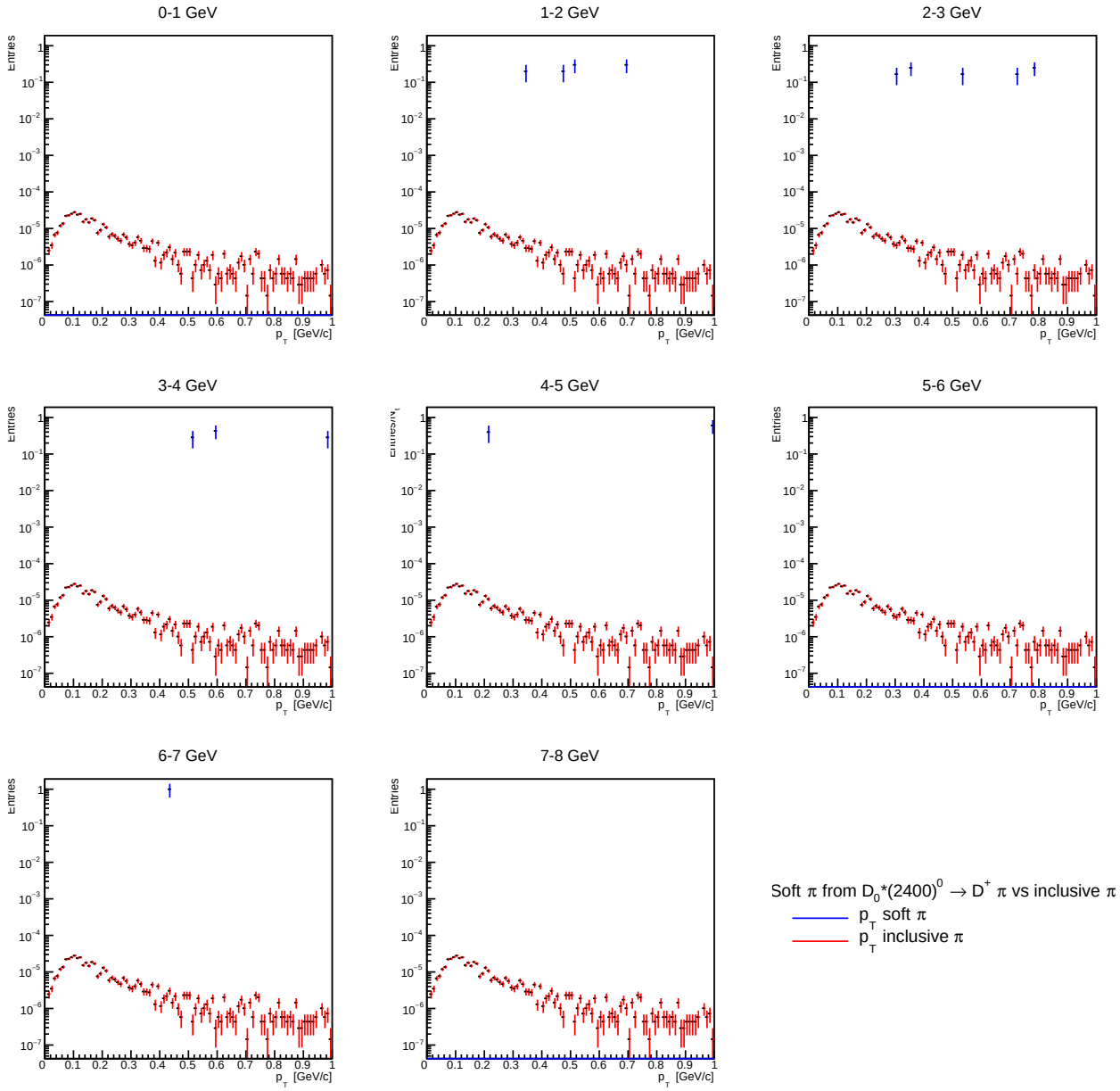

Figure 5.8: Soft pions $D_0^*(2400)^0$ versus inclusive pions p_T

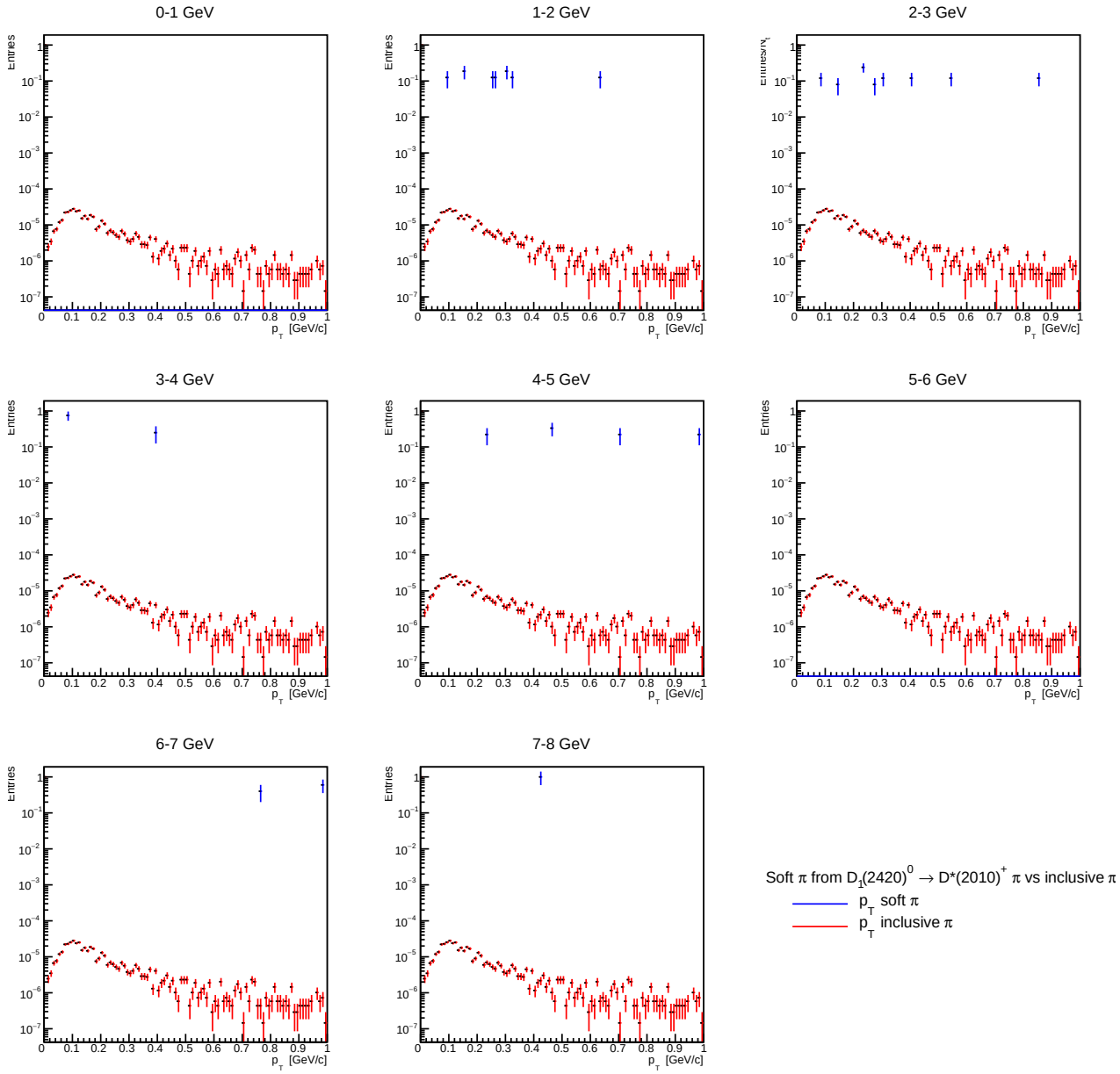

Figure 5.9: Soft pions $D_1(2420)^0$ versus inclusive pions p_T

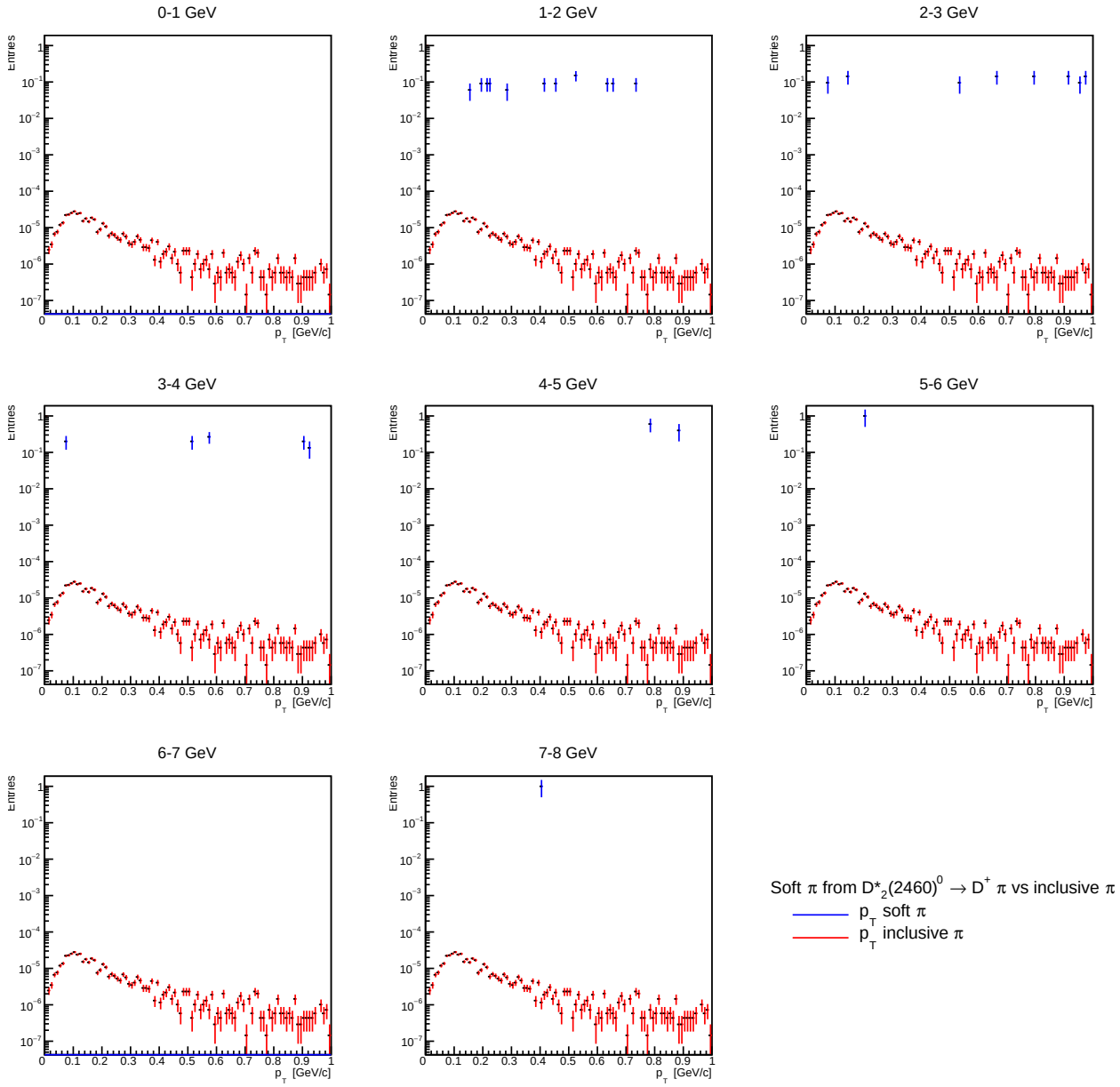

Figure 5.10: Soft pions $D_2^*(2460)^0$ versus inclusive pions p_T

The lowest p_T that can be measured by the ALICE detector is 100 MeV. In table tables 5.2, 5.3, 5.4, 5.5, the maximum and minimum p_T of the soft pions is shown and the percentage above 100 MeV. It can be seen that from p_T bins [1-2] onwards, the percentage is above 100 %, with a few exceptions. We can thus assume that only the D mesons with a p_T of higher than 1 to 2 GeV can be measured in the ALICE detector and reconstructed. This enables us to cut away background information which allows us to make data analysis more efficient.

$D^*(2010)^+$ p_T bins (GeV/c)	[0-1]	[1-2]	[2-3]	[3-4]	[4-5]	[5-6]	[6-7]	[7-8]	[8-9]
Max p_T (GeV/c)	0.005	0.105	0.155	0.295	0.295	0.325	0.425	0.445	0.495
Min p_T (GeV/c)	0.005	0.005	0.005	0.005	0.005	0.005	0.005	0.005	0.005
Percentage soft pions above 100 MeV (%)	0	62.1	98.9	100	100	100	100	100	100

Table 5.2: Maximum p_T, minimum p_T and the percentage of the soft pions of $D^*(2010)^+$ that is above 100 MeV.

$D_0^*(2400)^0$ p_T bins (GeV/c)	[0-1]	[1-2]	[2-3]	[3-4]	[4-5]	[5-6]	[6-7]	[7-8]	[8-9]
Max p_T (GeV/c)	0.005	0.515	0.355	0.595	0.995	0.005	0.435	0.005	0.005
Min p_T (GeV/c)	0.005	0.005	0.005	0.005	0.005	0.005	0.005	0.005	0.005
Percentage soft pions above 100 MeV (%)	0	100	100	100	100	0	100	0	0

Table 5.3: Maximum p_T, minimum p_T and the percentage of the soft pions of $D_0^*(2400)^0$ that is above 100 MeV.

$D_1(2420)^0$ p_T bins (GeV/c)	[0-1]	[1-2]	[2-3]	[3-4]	[4-5]	[5-6]	[6-7]	[7-8]	[8-9]
Max p_T (GeV/c)	0.005	0.155	0.235	0.085	0.465	0.005	0.985	0.425	0.005
Min p_T (GeV/c)	0.005	0.005	0.005	0.005	0.005	0.005	0.005	0.005	0.005
Percentage soft pions above 100 MeV (%)	0	87.5	89.3	40	100	100	100	100	100

Table 5.4: Maximum p_T, minimum p_T and the percentage of the soft pions of $D_1(2420)^0$ that is above 100 MeV.

$D_1^*(2460)^0$ p_T bins (GeV/c)	[0-1]	[1-2]	[2-3]	[3-4]	[4-5]	[5-6]	[6-7]	[7-8]	[8-9]
Max p_T (GeV/c)	0.005	0.525	0.145	0.757	0.785	0.205	0.005	0.405	0.005
Min p_T (GeV/c)	0.005	0.005	0.005	0.005	0.005	0.005	0.005	0.005	0.005
Percentage soft pions above 100 MeV (%)	0	100	92.9	88.9	100	100	100	100	100

Table 5.5: Maximum p_T, minimum p_T and the percentage of the soft pions of $D_2^*(2460)^0$ that is above 100 MeV.

Chapter 6

Discussion, Conclusion and outlook

6.1 Discussion and conclusion

The study presented in this thesis provides evidence that the reconstruction of higher D meson states with the ALICE detector during LHC run III is feasible. In table 5.1 it can be seen that, depending on the species, we can expect a range of a few millions to a few billions of D mesons produced within ALICE detector acceptance $|\eta| < 0.9$. Such numbers, even accounting for possible detector inefficiencies and acceptance effects of the order of 99% at low transverse momentum, give a reasonably safe number of D mesons in order to perform the reconstruction in LHC run III data sample.

An additional result of the study presented in this manuscript is the investigation of the minimal p_T reach that we can expect for each of the D mesons examined. In particular the results in tables 5.2, 5.3, 5.4, 5.2 provide evidence that due to the correlation between the various D mesons p_T and the p_T of their relative soft pions we cannot aim, in data, to reconstruct these particles below a p_T of 1-2 GeV/c. The aforementioned statement is driven from the fact that for $p_T <$ 1-2 GeV/c the p_T of the relative soft pions fall below the threshold of 100 MeV/c at which the ALICE detector is not able to track particles. This can be taken into account when reconstructing these mesons. However, it is important to note that in this study there were little statistics and therefore the uncertainties are large.

Furthermore, the study of the production vertexes of $D_0^*(2400)^0$, $D_1(2420)^0$ and $D_2^*(2460)^0$ is promising since this thesis shows evidence that a sizeable displacement from the primary interaction vertex takes place. This could imply that we could make cuts based on the mean decay lengths of the higher D^* meson states produced in the collision.

6.2 Outlook

As pointed out earlier, the uncertainties in this thesis are high. Further research should be done with a larger set of simulated events in order to minimize the uncertainties and affirm D mesons are feasible probes in the third LHC run. Furthermore, in figures 5.7, 5.8, 5.9, 5.10 for the soft pion p_T of each D meson state a table of cuts could be made stating how much of the background would be eliminated and how much of the signal would be lost.

Additional research could look into the production vertexes of the higher D^* meson states in more detail. They could investigate whether these D mesons are produced feed-down from B mesons. This could explain the wider spread production vertexes of the D mesons. Moreover, reconstruction cuts could be made depending on the mean decay length of the higher D^* meson states.

Next to that, further research could be done by investigating the invariant mass of the D mesons. Reconstructing the invariant mass would show us whether the peaks of the invariant mass would stand out from the background. Again this would enable us to make cuts on the background resulting in ALICE being able to more efficiently analyze the data from the third LHC run in order to perform the invariant mass analysis parametrizations of the expected ALICE p_T and $r\phi$ resolutions should be plugged in the PYTHIA simulation in order to reproduce the expected detector effects in the tracking.

References

[1] G. Aad et al. "The ATLAS experiment at the CERN large hadron collider." In: *Jinst* 3 (2008).

[2] Alice Collaboration. Abelev B. "Upgrade of the ALICE experiment: letter of intent." In: *Journal of Physics G: Nuclear and Particle Physics* 41(8) (2014).

[3] M. C. Abreu et al. "Anomalous J/ψ suppression in Pb-Pb interactions at 158 GeV per nucleon." In: *Physics Letters B* 410 (1997), pp. 337–343.

[4] CERN. *CMS observes melting of Upsilon particles in heavy-ion collisions*. `https://cms.cern/news/cms-observes-melting-upsilon-particles-heavy-ion-collisions`. Accessed on 08/07/20. 2012.

[5] CERN. *Home page*. `https://home.cern/`. Accessed on 06/03/20.

[6] CERN. *More details on the Time of Flight*. `http://alice.web.cern.ch/detectors/more-details-time-flight`. Accessed on 08/07/20.

[7] CERN. *ROOT Data Analysis Framework User's Guide*. `https://root.cern.ch/root/htmldoc/guides/users-guide/ROOTUsersGuide.html`. Accessed on 08/07/20. 2018.

[8] A. K. Chaudhuri. *A short course on relativistic heavy ion collisions*. IOP Publishing, 2014.

[9] ATLAS Collaboration et al. "Observation of a new particle in the search for the Standard Model Higgs boson with the ATLAS detector at the LHC". In: *Physics Letters B* 716 (2012), pp. 1–29.

[10] C. M. S. Collaboration. "The CMS experiment at the CERN LHC." In: *Institute of Physics Publishing and Sissa* (2008).

[11] LHCb Collaboration. "LHCb detector performance". In: *International Journal of Modern Physics A* 30(07) (2015), p. 1530022.

[12] ALICE collaboration. "Underlying event properties in pp collisions at s= 13 TeV." In: *Journal of High Energy Physics* 2020(4) (2020).

[13] L. Evans and P. Bryant. "LHC machine". In: *Journal of instrumentation* 3(08) (2008).

[14] C. Fabjan and J. Schukraft. "The story of ALICE: Building the dedicated heavy ion detector at LHC." In: *arXiv preprint arXiv:1101.1257.* (2011).

[15] S. D. Henley E. M. Eliss. *100 years of subatomic physics.* World Scientific, 2013.

[16] J. P. Iddon. "Commissioning of the new ALICE Inner Tracking System". In: *arXiv: 2005.01443* (2020).

[17] J. P. Iddon. "Commissioning of the new ALICE Inner Tracking System." In: *arXiv preprint arXiv:2005.01443.* (2020).

[18] V. A. Khoze et al. "Inelastic J/ψ and Υ hadroproduction." In: *The European Physical Journal C-Particles and Fields* 39(2) (2005), pp. 163–171.

[19] L. Kluberg. "20 years of J/ψ suppression at the CERN SPS, Results from Experiments NA38, NA51 and NA50". In: *Eur. Phys. J.* C 43 (2005), p. 145.

[20] Alice Collaboration. Kuijer P. "The inner tracking system of the Alice experiment." In: *Nuclear Instruments and Methods in Physics Research Section A: Accelerators, Spectrometers, Detectors and Associated Equipment* 530(1-2) (2004), pp. 28–32.

[21] C. Lippmann. "A continuous read-out TPC for the ALICE upgrade, conference proceedings." In: *Frontier Detectors for Frontier Physics–13th Pisa Meeting on Advanced Detectors* 27 (2015).

[22] F. Meddi. "The ALICE silicon pixel detector (SPD)." In: *Nuclear Instruments and Methods in Physics Research Section A: Accelerators, Spectrometers, Detectors and Associated Equipment* 465(1) (2001), pp. 40–45.

[23] B. Pullman. *The atom in the history of human thought.* Oxford University Press, 2001.

[24] T. Sjöstrand et al. "An introduction to PYTHIA 8.2." In: *Computer physics communications* 191 (2015), pp. 159–177.

[25] G. Stefanini. "Progress in the ALICE silicon pixel detector." In: *Nuclear Instruments and Methods in Physics Research Section A: Accelerators, Spectrometers, Detectors and Associated Equipment* 530(1-2) (2004), pp. 77–81.

[26] Alice Collaboration. Trzaska W. H. "New ALICE detectors for Run 3 and 4 at the CERN LHC." In: *Nuclear Instruments and Methods in Physics Research Section A: Accelerators, Spectrometers, Detectors and Associated Equipment* 958 (2020), p. 162116.

[27] R. Vogt. "New Temperature Probe for Quark-Gluon Plasma". In: *Physics* 5 (2012), p. 132.

[28] Sarah Webb. *Early-universe soup*. `https://i0.wp.com/deixismagazine.org/wp-content/uploads/2016/06/DOL_Plasma.png?ssl=1`. Accessed on 06/07/20.

[29] Wikipedia. *Standard model of elementary particles*. `https://upload.wikimedia.org/wikipedia/commons/0/00/Standard_Model_of_Elementary_Particles.svg`. Accessed on 06/07/20.

Appendix

Code used in macro for pp collision simulation.

The following code is part of the macro that saved information in a tree structure. Only $D_0^*(2400)^0$ is given as example, the other D mesons and inclusive pions were saved in the tree similarly.

```
#include "TSystem.h"
#include "TH1F.h"
#include "TClonesArray.h"
#include "TPythia8.h"
#include "TParticle.h"
#include "TDatabasePDG.h"
#include "TCanvas.h"
#include "TBranch.h"

void treefile(Int_t nev  =10000000,Int_t ndeb = 1)
{
  // Load libraries
 #ifndef G__WIN32 // Pythia8 is a static library on Windows
   if (gSystem->Getenv("PYTHIA8")) {
      gSystem->Load("$PYTHIA8/lib/libpythia8");
   } else {
      gSystem->Load("libpythia8");
   }
#endif
   gSystem->Load("libEG");
   gSystem->Load("libEGPythia8");
   //--------------------Declare variables--------------------------//
   Int_t np;

typedef struct {
  // PDG codes           D10421 = D*_0(2400)^0      D411 = D+    SoftPi
   = pion with low momentum from D^*(2400)^0 -> D+ pion
```

```
27  // PDG codes           K = kaon from D+ -> kaon pion        Pi = pion
    from D+ -> kaon pion
28    Int_t nD10421;
29    Float_t D10421_pt;
30    Float_t D10421_eta;
31    Float_t D10421_phi;
32    Float_t D10421_vx;
33    Float_t D10421_vy;
34    Float_t D10421_vz;
35    Float_t D411_pt;
36    Float_t D411_eta;
37    Float_t D411_phi;
38    Float_t D411_vx;
39    Float_t D411_vy;
40    Float_t D411_vz;
41    Float_t SoftPi_pt;
42    Float_t SoftPi_eta;
43    Float_t SoftPi_phi;
44    Float_t K_pt;
45    Float_t K_eta;
46    Float_t K_phi;
47    Float_t Pi_pt;
48    Float_t Pi_eta;
49    Float_t Pi_phi;
50  } d10421;
51
52
53 static d10421 D10421;
54
55   Float_t eta;
56   Float_t pt;
57
58   //-----------------Construction of the tree---------------------//
59   TFile* treefile = new TFile("treefile.root", "RECREATE");
60   TTree* tree = new TTree("tree", "tree");
61
62
63   //------- Make branch that saves kinematic properties of decay   D*
    _0(2400)^0 -> D+ pion  D+ -> kaon + pion -----------------//
64   tree -> Branch("D10421", &D10421, "nD10421/I:D10421_pt/F:D10421_eta/
    F:D10421_phi/F:D10421_vx/F:D10421_vy/F:D10421_vz/F:D411_pt/F:
    D411_eta/F:D411_phi/F:D411_vx/F:D411_vy/F:D411_vz/F:SoftPi_pt:
```

```
   SoftPi_eta:SoftPi_phi:K_pt:K_eta:K_phi:Pi_pt:Pi_eta:Pi_phi");
65
66
67 // Array of particles
68 TClonesArray* particles = new TClonesArray("TParticle", 1000);
69 // Create pythia8 object
70 TPythia8* pythia8 = new TPythia8();
71
72
73 // Configure
74 pythia8->ReadString("SoftQCD:all = on");
75
76 // ---------Force all D+ to decay in pion and kaon. Note BR for this
    decay becomes 100% ----------------------------//
77 pythia8->ReadString("411:onMode = off");
78 pythia8->ReadString("411:onIfMatch = 311 211");
79
80 //---------- Force all D0 to decay in pion and kaon. Note BR for
   this decay becomes 100% --------------------------//
81 pythia8->ReadString("421:onMode = off");
82 pythia8->ReadString("421:onIfMatch = 321 211");
83
84 //---------- Turn on all decays of D*_2(2460)^0 that contain D+.
   Note total BR for all decays containing D+ becomes 100% ---//
85 pythia8->ReadString("425:onMode = off");
86 pythia8->ReadString("425:onIfAny = 411");
87
88 //---------- Turn on all decays of D_1(2420)^0 that contain D*(2010)
   ^+. Note total BR for all decays containing D*(2010)^+ becomes 100%
   ---//
89 pythia8->ReadString("10423:onMode = off");
90 pythia8->ReadString("10423:onIfAny = 413");
91
92 // Initialize
93 pythia8->Initialize(2212 /* p */, 2212 /* p */, 13000. /* TeV */);
94
95 //--------------------------- Event loop-------------------------//
96 for (Int_t iev = 0; iev < nev; iev++) {
97 Int_t nDstar0 = 0;
98
99 // Initialialize variable
100 D10421.nD10421 = -9;
```

```
101
102   pythia8->GenerateEvent();
103   if (iev < ndeb) pythia8->EventListing();
104   pythia8->ImportParticles(particles,"All");
105   np = particles->GetEntriesFast();
106   if(np<8) continue;
107
108   //------------------------ Particle loop-----------------------//
109      for (Int_t ip = 0; ip < np; ip++) {
110
111       // Initialize variables
112       D10421.D10421_pt = -9;
113       D10421.D10421_eta =  -20;
114       D10421.D10421_phi = -20;
115       D10421.D10421_vx = -20;
116       D10421.D10421_vy = -20;
117       D10421.D10421_vz = -20;
118       D10421.D411_pt = -9;
119       D10421.D411_eta =  -20;
120       D10421.D411_phi = -20;
121       D10421.D411_vx = -20;
122       D10421.D411_vy = -20;
123       D10421.D411_vz = -20;
124       D10421.SoftPi_pt = -9;
125       D10421.SoftPi_eta =  -20;
126       D10421.SoftPi_phi = -20;
127       D10421.K_pt = -9;
128       D10421.K_eta =  -20;
129       D10421.K_phi = -20;
130       D10421.Pi_pt = -9;
131       D10421.Pi_eta =  -20;
132       D10421.Pi_phi = -20;
133
134       TParticle* part = (TParticle*) particles->At(ip);
135       Int_t pdg = part->GetPdgCode();
136       if(pdg == 990 || (pdg <= 200 && pdg>=-200)) continue;
137
138       //Get the charge of the particle
139       TDatabasePDG* pdgBase = TDatabasePDG::Instance();
140       TParticlePDG *particle = pdgBase->GetParticle(pdg);
141       if(particle == NULL) continue;
142
```

```
143         //Speeds up selection process of the D mesons
144         if((pdg <= 400 && pdg>=-400)) continue;
145         if((pdg >=500 && pdg < 9000) || (pdg<=-500 && pdg > -9000))
    continue;
146         if(part->Pt()<1) continue;
147 
148         // Selection of D*_0(2400)^0 -> D+  pion
149             if (TMath::Abs(pdg) == 10421) {
150             Int_t Nd = part->GetNDaughters();
151              if(Nd ==2){
152              Int_t Dau1 = part->GetDaughter(0);
153              Int_t Dau2 = part->GetDaughter(1);
154              TParticle* firstD = (TParticle*) particles->At(Dau1);
155              Int_t pdg1D = firstD->GetPdgCode();
156              TParticle* secondD = (TParticle*) particles->At(Dau2);
157              Int_t pdg2D = secondD->GetPdgCode();
158              Int_t Nd2 = firstD->GetNDaughters();
159                  if(Nd2 == 2 && (TMath::Abs(pdg1D) == 411 || TMath::Abs(
    pdg1D) == 211) && (TMath::Abs(pdg2D) == 211 || TMath::Abs(pdg2D) ==
    411)) {              Int_t Dau2_1 = firstD ->GetDaughter(0);
160                 Int_t Dau2_2 = firstD ->GetDaughter(1);
161                 TParticle* firstD_2 = (TParticle*) particles->At(Dau2_1
    );
162                 Int_t pdg1D_2 = firstD_2->GetPdgCode();
163                 TParticle* secondD_2 = (TParticle*) particles->At(
    Dau2_2);
164                 Int_t pdg2D_2 = secondD_2->GetPdgCode();
165 
166                 // Selection of D+ -> kaon + pion
167                         if((TMath::Abs(pdg1D_2) == 311 || TMath::Abs(
    pdg1D_2) == 211) && (TMath::Abs(pdg2D_2) == 211 || TMath::Abs(
    pdg2D_2) == 311)) {                    nDstar0 = nDstar0+1;
168                           // Save kinematic properties of D*_0(2400)^0
169                           D10421.D10421_pt = part -> Pt();
170                           D10421.D10421_eta =  part->Eta();
171                           D10421.D10421_phi = part->Phi();
172                           D10421.D10421_vx = part->Vx();
173                           D10421.D10421_vy = part->Vy();
174                           D10421.D10421_vz = part->Vz();
175                           // Save kinematic properties of D+
176                           D10421.D411_pt = firstD->Pt();
177                           D10421.D411_eta =  firstD->Eta();
```

```
178                          D10421.D411_phi = firstD->Phi();
179                          D10421.D411_vx = firstD->Vx();
180                          D10421.D411_vy = firstD->Vy();
181                          D10421.D411_vz = firstD->Vz();
182                          // Save kinematic properties of pion from D
   ^*(2400)^0 -> D+ pion
183                          D10421.SoftPi_pt = secondD->Pt();
184                          D10421.SoftPi_eta =  secondD->Eta();
185                          D10421.SoftPi_phi = secondD->Phi();
186
187                          if(TMath::Abs(pdg1D_2) ==311){
188                            // Save kinematic properties of kaon from D
   + -> kaon pion
189                            D10421.K_pt = firstD_2->Pt();
190                            D10421.K_eta =  firstD_2->Eta();
191                            D10421.K_phi = firstD_2->Phi();
192                            D10421.Pi_pt = secondD_2->Pt();
193                            D10421.Pi_eta =  secondD_2->Eta();
194                            D10421.Pi_phi = secondD_2->Phi();
195                          }else{
196                            // Save kinematic properties of pion from D
   + -> kaon pion
197                            D10421.Pi_pt = firstD_2->Pt();
198                            D10421.Pi_eta =  firstD_2->Eta();
199                            D10421.Pi_phi = firstD_2->Phi();
200                            D10421.K_pt = secondD_2->Pt();
201                            D10421.K_eta =  secondD_2->Eta();
202                            D10421.K_phi = secondD_2->Phi();
203                               }
204                        }
205                 }
206           }
207           }
208     D10421.nD10421 = nDstar0;
209     tree->Fill();
210     }
211    tree->Print();
212    tree -> Write();
213 }
```

The code given below is part of the macro that read information from a tree structure to plot histograms.

```
#include "TFile.h"
#include "TTree.h"
#include "TBranch.h"
#include "TH1F.h"

void treereader(){
  //------------------------ Define histograms --------------------//
   //Histogram pseudorapidity
   TH1F* D10421_etaH = new TH1F("D10421_etaH", "D10421_eta", 120, -12., 12.);

   //Histograms transverse momentum
   TH1F* D10421_ptH = new TH1F("D10421_ptH", "D10421_ptH", 20, 0., 20.);
   TH1F* D10421_D411_ptH = new TH1F("D10421_D411_ptH", "D10421_D411_ptH", 20, 0., 20.);
   TH1F* D10421_SoftPi_ptH = new TH1F("D10421_SoftPi_ptH", "D10421_SoftPi_ptH", 100, 0., 4.);
   TH1F* D10421_SoftPi_02= new TH1F("D10421_SoftPi_02", "D10421_SoftPi_02", 100, 0., 1.);
   TH1F* D10421_SoftPi_24 = new TH1F("D10421_SoftPi_24", "D10421_SoftPi_24", 100, 0., 1.);
   TH1F* D10421_SoftPi_46 = new TH1F("D10421_SoftPi_46", "D10421_SoftPi_46", 100, 0., 1.);
   TH1F* D10421_SoftPi_68 = new TH1F("D10421_SoftPi_68", "D10421_SoftPi_68", 100, 0., 1.);
   TH1F* D10421_SoftPi_810 = new TH1F("D10421_SoftPi_810", "D10421_SoftPi_810", 100, 0., 1.);
   TH1F* D10421_SoftPi_1012 = new TH1F("D10421_SoftPi_1012", "D10421_SoftPi_1012", 100, 0., 1.);
   TH1F* D10421_SoftPi_1214 = new TH1F("D10421_SoftPi_1214", "D10421_SoftPi_1214", 100, 0., 1.);
   TH1F* D10421_SoftPi_1416 = new TH1F("D10421_SoftPi_1416", "D10421_SoftPi_1416", 100, 0., 1.);
   TH1F* D10421_SoftPi_1618 = new TH1F("D10421_SoftPi_1618", "D10421_SoftPi_1618", 100, 0., 1.);
   TH1F* D10421_K_ptH = new TH1F("D10421_K_pt","D10421_K_ptH", 20, 0., 20.);
   TH1F* D10421_Pi_ptH = new TH1F("D10421_Pi_ptH", "D10421_Pi_ptH", 20, 0., 20.);

   //Histogram for correlation D*_0(2400)^0 vs  pion from decay D*_0
```

```
   (2400)^0 -> D+ pion
   TH2F* D10421_correlationH = new TH2F("D10421_correlationH", "
   D10421_correlationH", 200, 0., 20., 200, 0., 4.);

   //Histogram production vertex
   TH2F* D10421_vxyH = new TH2F("D10421_vxyH", "D10421_vxyH", 100, -4.,
    4., 100, -4., 4.);

   //------------------------ Read out tree ------------------------//

   //---------------------- Declare variables ----------------------//
   // PDG codes           D10421 = D*_0(2400)^0      D411 = D+    SoftPi
    = pion with low momentum from D^*(2400)^0 -> D+ pion
   // PDG codes           K = kaon from D+ -> kaon pion        Pi = pion
    from D+ -> kaon pion
typedef struct {
     Int_t nD10421;
     Float_t D10421_pt;
     Float_t D10421_eta;
     Float_t D10421_phi;
     Float_t D10421_vx;
     Float_t D10421_vy;
     Float_t D10421_vz;
     Float_t D411_pt;
     Float_t D411_eta;
     Float_t D411_phi;
     Float_t D411_vx;
     Float_t D411_vy;
     Float_t D411_vz;
     Float_t SoftPi_pt;
     Float_t SoftPi_eta;
     Float_t SoftPi_phi;
     Float_t K_pt;
     Float_t K_eta;
     Float_t K_phi;
     Float_t Pi_pt;
     Float_t Pi_eta;
     Float_t Pi_phi;
   } d10421;

   static d10421 D10421;

```

```
65    Int_t D10421_above100_02 = 0;
66    Int_t D10421_above100_24 = 0;
67    Int_t D10421_above100_46 = 0;
68    Int_t D10421_above100_68 = 0;
69    Int_t D10421_above100_810 = 0;
70    Int_t D10421_above100_1012 = 0;
71    Int_t D10421_above100_1214 = 0;
72    Int_t D10421_above100_1416 = 0;
73    Int_t D10421_above100_1618 = 0;
74
75    // Getting tree
76    TFile *treefile = new TFile("10millionevents.root");
77    TTree *tree = (TTree*)treefile -> Get("tree");
78    TBranch *D10421_branch = tree -> GetBranch("D10421");
79    D10421_branch -> SetAddress(&D10421);
80
81    // Filling histograms
82    Long64_t nentries = tree -> GetEntries();
83    for(Long64_t i =0; i<nentries; i++)
84      {
85      D10421_branch -> GetEntry(i);
86      // Select only the statistics in pseudorapidity range |eta|<0.9
87      if(TMath::Abs(D10421.D10421_eta)<0.9){
88      if(D10421.nD10421>0){ totalD10421 +=  D10421.nD10421;}
89      D10421_ptH -> Fill(D10421.D10421_pt);
90      D10421_D411_ptH -> Fill(D10421.D411_pt);
91      D10421_SoftPi_ptH -> Fill(D10421.SoftPi_pt);
92      if(D10421.D10421_pt>0 && D10421.D10421_pt<1) D10421_SoftPi_02 ->
    Fill(D10421.SoftPi_pt);
93      if(D10421.D10421_pt>1 && D10421.D10421_pt<2) D10421_SoftPi_24 ->
    Fill(D10421.SoftPi_pt);
94      if(D10421.D10421_pt>2 && D10421.D10421_pt<3) D10421_SoftPi_46 ->
    Fill(D10421.SoftPi_pt);
95      if(D10421.D10421_pt>3 && D10421.D10421_pt<4) D10421_SoftPi_68 ->
    Fill(D10421.SoftPi_pt);
96      if(D10421.D10421_pt>4 && D10421.D10421_pt<5) D10421_SoftPi_810 ->
    Fill(D10421.SoftPi_pt);
97      if(D10421.D10421_pt>5 && D10421.D10421_pt<6) D10421_SoftPi_1012 ->
     Fill(D10421.SoftPi_pt);
98      if(D10421.D10421_pt>6 && D10421.D10421_pt<7) D10421_SoftPi_1214 ->
     Fill(D10421.SoftPi_pt);
99      if(D10421.D10421_pt>7 && D10421.D10421_pt<8) D10421_SoftPi_1416 ->
```

```
    Fill(D10421.SoftPi_pt);
100     if(D10421.D10421_pt>8 && D10421.D10421_pt<9) D10421_SoftPi_1618 ->
    Fill(D10421.SoftPi_pt);
101     if(D10421.D10421_pt>0 && D10421.D10421_pt<1 && D10421.SoftPi_pt
    >0.1) D10421_above100_02++;
102     if(D10421.D10421_pt>1 && D10421.D10421_pt<2 && D10421.SoftPi_pt
    >0.1) D10421_above100_24++;
103     if(D10421.D10421_pt>2 && D10421.D10421_pt<3 && D10421.SoftPi_pt
    >0.1) D10421_above100_46++;
104     if(D10421.D10421_pt>3 && D10421.D10421_pt<4 && D10421.SoftPi_pt
    >0.1) D10421_above100_68++;
105     if(D10421.D10421_pt>4 && D10421.D10421_pt<5 && D10421.SoftPi_pt
    >0.1) D10421_above100_810++;
106     if(D10421.D10421_pt>5 && D10421.D10421_pt<6 && D10421.SoftPi_pt
    >0.1) D10421_above100_1012++;
107     if(D10421.D10421_pt>6 && D10421.D10421_pt<7 && D10421.SoftPi_pt
    >0.1) D10421_above100_1214++;
108     if(D10421.D10421_pt>7 && D10421.D10421_pt<8 && D10421.SoftPi_pt
    >0.1) D10421_above100_1416++;
109     if(D10421.D10421_pt>8 && D10421.D10421_pt<9 && D10421.SoftPi_pt
    >0.1) D10421_above100_1618++;
110     D10421_K_ptH -> Fill(D10421.K_pt);
111     D10421_Pi_ptH -> Fill(D10421.Pi_pt);
112     D10421_etaH -> Fill(D10421.D10421_eta);
113     D10421_vxyH -> Fill(D10421.D10421_vx, D10421.D10421_vy);}
114       }
115 }
```